

This work was written as part of one of the author's official duties as an Employee of the United States Government and is therefore a work of the United States Government. In accordance with 17 U.S.C. 105, no copyright protection is available for such works under U.S. Law.

Public Domain Mark 1.0

<https://creativecommons.org/publicdomain/mark/1.0/>

Access to this work was provided by the University of Maryland, Baltimore County (UMBC) ScholarWorks@UMBC digital repository on the Maryland Shared Open Access (MD-SOAR) platform.

**Please provide feedback**

Please support the ScholarWorks@UMBC repository by emailing [scholarworks-group@umbc.edu](mailto:scholarworks-group@umbc.edu) and telling us what having access to this work means to you and why it's important to you. Thank you.

## SOLAR WIND MODELING WITH TURBULENCE TRANSPORT AND HEATING

ARCADI V. USMANOV<sup>1,2</sup>, WILLIAM H. MATTHAEUS<sup>2</sup>, BENJAMIN A. BREECH<sup>3</sup>, AND MELVYN L. GOLDSTEIN<sup>1</sup>

<sup>1</sup> Code 673, NASA Goddard Space Flight Center, Greenbelt, Maryland 20771, USA; [arcadi.usmanov@nasa.gov](mailto:arcadi.usmanov@nasa.gov)

<sup>2</sup> Department of Physics and Astronomy and Bartol Research Institute, University of Delaware, Newark, DE 19716, USA

<sup>3</sup> NASA Postdoctoral Program, Goddard Space Flight Center, Greenbelt, Maryland 20771, USA

Received 2010 September 13; accepted 2010 November 18; published 2011 January 6

### ABSTRACT

We have developed an axisymmetric steady-state solar wind model that describes properties of the large-scale solar wind, interplanetary magnetic field, and turbulence throughout the heliosphere from 0.3 AU to 100 AU. The model is based on numerical solutions of large-scale Reynolds-averaged magnetohydrodynamic equations coupled with a set of small-scale transport equations for the turbulence energy, normalized cross helicity, and correlation scale. The combined set of time-dependent equations is solved in the frame of reference corotating with the Sun using a time-relaxation method. We use the model to study the self-consistent interaction between the large-scale solar wind and smaller-scale turbulence and the role of the turbulence in the large-scale structure and temperature distribution in the solar wind. To illuminate the roles of the turbulent cascade and the pickup protons in heating the solar wind depending on the heliocentric distance, we compare the model results with and without turbulence/pickup protons. The variations of plasma temperature in the outer heliosphere are compared with *Ulysses* and *Voyager 2* observations.

**Key words:** magnetohydrodynamics (MHD) – methods: numerical – solar wind – turbulence

### 1. INTRODUCTION

The physical processes that determine the structure and properties of the solar wind have been under study since Parker first published his theory (Parker 1958). A large difference in thermal pressure between the coronal and interstellar plasma led Parker to predict that the solar corona streams outward to form a wind that becomes supersonic at a few solar radii. Parker’s theory implied a source of internal energy that extended far out into space. Originally, to account implicitly for this source, Parker postulated that the solar corona was isothermal up to some distance from the Sun. Later he employed a polytropic energy equation with polytropic index  $\gamma \neq 5/3$  as a proxy for the non-adiabatic energy transport and demonstrated that in the framework of that model, solar-wind-type (transonic) solutions do not exist for  $\gamma = 5/3$  (Parker 1960). Subsequent spacecraft observations have confirmed the existence of the supersonic solar wind (Neugebauer & Snyder 1962) and that it cools with distance at a rate that is significantly slower than the adiabatic rate (Smith & Wolfe 1979; Marsch et al. 1981; Gazis & Lazarus 1982). However, the sources of the internal energy needed to establish this non-adiabatic expansion have remained uncertain.

Spacecraft observations have also revealed that the solar wind is often structured into a slow wind ( $\sim 300\text{--}400\text{ km s}^{-1}$ ) that is usually relatively variable and dense, and a fast wind ( $\sim 700\text{--}800\text{ km s}^{-1}$ ) that is typically more steady and tenuous (e.g., Phillips et al. 1995). The fast solar wind is known to originate in coronal holes that are associated with unipolar magnetic field, while the slow wind is typically observed in the vicinity of magnetic sector boundaries (Balogh et al. 1995). The characteristics of slow wind are relatively easy to replicate in Parker’s polytropic model (e.g., Leer et al. 1982). On the other hand, to reproduce the fast wind, an additional source of thermal energy or momentum must be included in Parker’s equations (Munro & Jackson 1977; Leer et al. 1982; Barnes et al. 1995). Otherwise, models invariably predict a ratio of 1 AU density to

a coronal base density that is too high (Hundhausen 1972; Leer et al. 1982).

The overwhelming majority of models of the solar wind employ a non-adiabatic polytrope (see, for example, the three-dimensional models by Linker et al. 1990; Usmanov 1993a, 1993b; Mikić & Linker 1996; Linker et al. 1999; Riley et al. 2001; Roussev et al. 2003; Hayashi 2005; Cohen et al. 2007). Other models introduce ad hoc source functions into the energy equation (Groth et al. 2000; Nakamizo et al. 2009). The non-adiabatic polytropic index  $\gamma$  for the solar wind is usually calibrated using spacecraft observations (e.g.,  $\gamma = 1.17$  by Sittler & Scudder (1980) from *Voyager 2* and *Mariner 10* data,  $\gamma = 1.46$  by Totten et al. (1995) from *Helios* proton data, or  $\gamma = 1.28$  by Whang (1998) from *Voyager 2* data).

Parker’s non-adiabatic index implies an unspecified source of internal energy for each flow element. Close to the Sun, where magnetic forces dominate over the sub-Alfvénic coronal expansion, the magnetic field is capable of redistributing the energy around the Sun to produce higher outflow speeds in open field regions and slower wind above closed field structures (e.g., Pneuman & Kopp 1971; Steinolfson et al. 1982). However, to generate the observed fast-slow wind contrast, an additional mechanism is required that deposits momentum/energy primarily into the fast wind. The physics of this mechanism is not well understood.

The solar wind is a weakly collisional plasma composed primarily of electrons and protons, with a small admixture ( $\sim 5\%$ ) of heavier ions, mostly ionized helium. The electrons and protons generally have notably different temperatures. While the protons in fast wind are typically about twice as hot as the electrons (e.g., Feldman et al. 1996), protons are usually colder than the electrons in slow wind (Hundhausen 1972). One source of heat to the solar wind arises from thermal conduction from the  $10^6\text{ K}$  corona that is carried primarily by electrons. Another source of heat is provided by the dissipation of waves and/or turbulent fluctuations in the solar wind (see, e.g., Axford & McKenzie 1992; Verma 1996; Matthaeus et al. 1999). If

the fluctuations are responsible for the added dissipation and heating, how does this occur and how large an effect is it?

Turbulent fluctuations over a wide range of temporal and spatial scales are ubiquitous in the solar wind (see, e.g., the reviews by Goldstein et al. 1995; Bruno & Carbone 2005). In fast wind, the turbulence has the appearance of large-amplitude Alfvénic fluctuations that propagate away from the Sun (Unti & Neugebauer 1968; Belcher & Davis 1971). In slow wind, the fluctuations are typically less Alfvénic (i.e., the velocity and magnetic field variations are less correlated) and, consequently, the dominance of outward propagation is reduced. Because the fast-wind Alfvénic correlations suggest outward propagation, it is natural to assume that their source resides on the Sun or inner corona, below the Alfvénic critical point. The fluctuations cascade, dissipate, and heat the corona and solar wind. The turbulent heating typically leads to an increased outward thermal pressure gradient, and therefore to an indirect acceleration of the wind. The fluctuations are also able to accelerate the bulk flow directly by outward wave pressure gradient (ponderomotive force) even in the absence of wave damping (Belcher 1971; Alazraki & Couturier 1971).

There are two approaches to model the evolution of fluctuations in the solar wind. The first is based on a statistical description of fluctuations, using, e.g., the short-wavelength Wentzel–Kramers–Brillouin (WKB) approximation (Belcher 1971; Alazraki & Couturier 1971), non-WKB two-scale decomposition (Marsch & Tu 1989; Zhou & Matthaeus 1990), large eddy simulation (LES; Shimomura 1991; Chernyshov et al. 2006, 2007), or Reynolds decomposition and averaging to follow large scales together with evolution/transport equations that describe unresolved small-scale effects of turbulence. The second approach is direct numerical simulation (DNS) of the magnetohydrodynamic (MHD) equations with explicit accounting for injection, propagation, and evolution of the fluctuations. While the statistical description is computationally less intense than DNS, it requires a closure condition, i.e., the equations contain terms that require separate modeling. On the other hand, while DNS avoids the closure problem, it is challenging due to computational speed and memory requirements. For the foreseeable future, direct multi-dimensional high-resolution numerical simulations of the solar wind will be unable to compute accurately both large-scale expansion and small-scale turbulence (e.g., Yokoi et al. 2008). Thus, it appears reasonable to turn to a statistical small-scale modeling approach to incorporate the physical effects of small-scale MHD turbulence into a large-scale MHD solar wind model.

The simplest statistical approach to account for the effects of noninteracting Alfvén waves is to apply the short-wavelength WKB approximation (e.g., Dewar 1970; Belcher 1971; Jacques 1977; Hollweg 1990). This approach permits a model to include effects of waves on the background flow and vice versa. The WKB approximation was extensively exploited in one-dimensional models with specified flow tube geometries (e.g., Jacques 1978; Hollweg 1978; Esser et al. 1986; Wang 1993) and proved that waves can provide additional acceleration. WKB wave acceleration was incorporated in two- and three-dimensional solar wind models by Usmanov (1996), Usmanov et al. (2000), and Usmanov & Goldstein (2003). The models demonstrated an agreement with the Wang–Sheeley empirical model (Wang & Sheeley 1990; Wang et al. 1997) and reproduced a bimodal solar wind structure consistent with *Ulysses* observations. The WKB wave-driven approach was lately implemented in a number of two- and three-dimensional solar wind models

(e.g., Chen & Hu 2001; Hu et al. 2003; Li et al. 2004; Lionello et al. 2009).

The models of Usmanov et al. produced useful results, but continued to employ a non-adiabatic polytropic index and ad hoc heating terms. Furthermore, WKB theory is unable to account for any sunward propagating waves and it predicts an equipartition of kinetic and magnetic fluctuation energy, while the observed magnetic energy is usually twice the kinetic energy (e.g., Matthaeus & Goldstein 1982; Yokoi et al. 2008). Also, WKB waves are noninteracting, which allows for neither turbulent cascades nor self-consistent heating.

In the present study, we relax the WKB approximation in the super-Alfvénic flow region and address the physical origin of the non-adiabatic polytrope by (1) incorporating Hollweg’s “collisionless” approximation for the electron heat flux (Hollweg 1974, 1976) into the energy equation and by (2) employing turbulence transport theory to describe statistically the effects of the transport, cascade, and dissipation of MHD turbulence (Zhou & Matthaeus 1990; Matthaeus et al. 1994; Hossain et al. 1995; Zank et al. 1996; Matthaeus et al. 1996b, 1999; Smith et al. 2001; Isenberg et al. 2003; Matthaeus et al. 2004; Smith et al. 2006; Breech et al. 2008; Isenberg et al. 2010; Yokoi 2010). In the theory, a phenomenological description of turbulent cascade is merged with transport equations to describe turbulence in a weakly inhomogeneous system such as the scale-separated solar wind (Marsch & Tu 1989; Zhou & Matthaeus 1990; Marsch & Tu 1993; Tu & Marsch 1993; Matthaeus et al. 1994). Initial two-equation turbulence transport theory (Zhou & Matthaeus 1990; Matthaeus et al. 1994; Zank et al. 1996; Matthaeus et al. 1996b) has evolved to include temperature effects (Matthaeus et al. 1999; Smith et al. 2001), cross-helicity effects (Matthaeus et al. 2004; Breech et al. 2005; Yokoi 2010), electron effects (Breech et al. 2009), and more recently the solar wind deceleration by pickup protons (Isenberg et al. 2010). With the selection of appropriate pickup ion driving, shear constants, and boundary values, the transport theory has been able to quantitatively account for *Helios* and *Ulysses* proton temperature observations (Matthaeus et al. 2004) as well as *Voyager* data from 1 to more than 60 AU (Zank et al. 1996; Matthaeus et al. 1999; Smith et al. 2001, 2006). Breech et al. (2008) applied the turbulence transport theory to an axially symmetric heliosphere with a constant speed and specified large-scale solar wind properties. Integrating one-dimensional turbulence transport equations along a number of radial lines with latitudinally varying boundary data inferred from observations, Breech et al. obtained a distribution of turbulence throughout the heliosphere.

In this paper, we attempt to bridge the gap between large-scale solar wind modeling and transport studies of small-scale turbulence by developing a model that is based on a self-consistent solution of the combined set of solar wind and turbulence transport equations. By including the turbulence transport model in a self-consistent way in our large-scale solar wind model, we are able to understand details of how turbulence influences the heating and large-scale solar wind properties and how the large-scale structure and properties of the solar wind affect the distribution of turbulence throughout the heliosphere.

To develop the model and achieve the required separation of small- and large-scale dynamical effects, we employ a straightforward Reynolds-averaging scheme. This may be regarded as a significant step beyond the WKB theory of noninteracting waves that has been more traditional in solar wind research. However, from a turbulence modeling perspective the present

approach cannot be regarded as complete because the large-scale flow fields can in principle directly lose energy to small scales through cascade. This direct contribution to the “eddy viscosity” is not captured by Reynolds-averaging method. To include such effects would therefore require an extension such as a spectral theory of eddy viscosity (Lesieur et al. 2005) or use of a multiple averaging scheme (e.g., Germano et al. 1991). This is beyond the scope of the present paper but may be a fruitful direction for future efforts in multiple scale solar wind simulation.

An important restriction of the present study is that the heliospheric structure is assumed to be north–south and axially symmetric. This assumption is appropriate for the solar wind structure near solar minimum when the large-scale magnetic field on the Sun can be approximated by a dipole aligned with the solar rotation axis and the solar wind consists of a slow belt near the helioequator and fast wind streams at higher latitudes. The axial symmetry also implies that we neglect the longitudinal dependence of the interstellar neutral hydrogen effect on the heliospheric structure.

The plan of the paper is as follows: in Section 2, we describe the governing equations and discuss in detail the initial and boundary conditions used. The results of the simulation are discussed in Section 3, which also contains a comparison of the model calculations with *Ulysses* and *Voyagers 2* data. A summary in Section 4 concludes the paper.

## 2. MODEL FORMULATION

In this paper, we apply the traditional one-fluid description of the solar wind as a fully ionized plasma, composed of comoving electrons and protons, and assume the number density  $\tilde{n} = n_p = n_e$  (charge neutrality), the temperature  $\tilde{T} = T_p = T_e$ , and the pressure  $\tilde{P} = P_p + P_e = \tilde{n}k_B(T_p + T_e)$ , where subscripts  $p$  and  $e$  refer to electrons and protons, respectively, and  $k_B$  is Boltzmann’s constant. We neglect the electron mass  $m_e$  compared to the proton mass  $m_p$ , so that the mass density  $\tilde{\rho} = nm_p$ .

The single-fluid ideal MHD equations describing the solar wind plasma and magnetic field in the frame of reference corotating with the Sun can be written in the form

$$\frac{\partial \tilde{\rho}}{\partial t} + \nabla \cdot (\tilde{\rho} \tilde{\mathbf{v}}) = 0, \quad (1)$$

$$\tilde{\rho} \left[ \frac{\partial \tilde{\mathbf{v}}}{\partial t} + (\tilde{\mathbf{v}} \cdot \nabla) \tilde{\mathbf{v}} \right] - \frac{1}{4\pi} (\nabla \times \tilde{\mathbf{B}}) \times \tilde{\mathbf{B}} + \nabla \tilde{P} + \tilde{\rho} \left[ \frac{GM_\odot}{r^2} \hat{\mathbf{r}} + 2\boldsymbol{\Omega} \times \tilde{\mathbf{v}} + \boldsymbol{\Omega} \times (\boldsymbol{\Omega} \times \mathbf{r}) \right] = 0, \quad (2)$$

$$\frac{\partial \tilde{\mathbf{B}}}{\partial t} = \nabla \times (\tilde{\mathbf{v}} \times \tilde{\mathbf{B}}), \quad (3)$$

$$\frac{\partial \tilde{P}}{\partial t} + (\tilde{\mathbf{v}} \cdot \nabla) \tilde{P} + \gamma \tilde{P} (\nabla \cdot \tilde{\mathbf{v}}) = -(\gamma - 1) \nabla \cdot \mathbf{q}_H + Q(\mathbf{r}), \quad (4)$$

where  $t$  is the time and  $\mathbf{r}$  is the heliocentric position vector. The dependent variables  $\tilde{\rho}$ ,  $\tilde{\mathbf{v}}$ ,  $\tilde{\mathbf{B}}$ , and  $\tilde{P}$  are the plasma density, the flow velocity in the corotating frame, the magnetic field, and the thermal pressure, respectively.  $M_\odot$  is the solar mass,  $\boldsymbol{\Omega}$  is the solar angular velocity vector,  $G$  is the gravitational constant,  $\hat{\mathbf{r}}$  is a unit vector in the radial direction, and  $\gamma$  is the ratio of specific heats. In addition to the inertial, Lorentz, thermal pressure gradient, and gravitational forces, the momentum

Equation (2) includes the Coriolis and the centrifugal forces. The pressure (energy) Equation (4) contains the heat conduction flux density  $\mathbf{q}_H$  that we will approximate by Hollweg’s “collisional” expression (Section 2.5) and a source term  $Q(\mathbf{r})$  that we will attribute to turbulent dissipation (Section 2.2).

### 2.1. Large-scale (Reynolds-averaged) Equations

To account for turbulence effects, we apply the Reynolds decomposition to Equations (1)–(4) by splitting the dependent variables into large-scale (ensemble average) and small-scale (fluctuating) components  $\tilde{\mathbf{a}} = \mathbf{a} + \mathbf{a}'$  according to the rule  $\mathbf{a} = \langle \tilde{\mathbf{a}} \rangle$ ,  $\langle \mathbf{a}' \rangle = 0$ , where  $\mathbf{a}$  is any of the physical variables and  $\langle \cdot \cdot \cdot \rangle$  is the ensemble average. In the present study, we assume that  $\rho' \equiv 0$ , i.e., that the small-scale turbulence is locally incompressible, while the large-scale flows are fully compressible. We will temporarily retain, however, terms involving  $P'$  to show how such effects might enter for next order theories of “near incompressibility.” By applying the ensemble averaging to Equations (1)–(4), we arrive at the following large-scale Reynolds-averaged equations:

$$\frac{\partial \rho}{\partial t} + \nabla \cdot (\rho \mathbf{v}) = 0, \quad (5)$$

$$\begin{aligned} \frac{\partial (\rho \mathbf{v})}{\partial t} + \nabla \cdot \left[ \rho \mathbf{v} \mathbf{v} - \frac{1}{4\pi} \mathbf{B} \mathbf{B} + \left( P + \frac{B^2}{8\pi} + \frac{\langle B'^2 \rangle}{8\pi} \right) \mathbf{I} \right. \\ \left. + \langle \rho \mathbf{v}' \mathbf{v}' - \frac{1}{4\pi} \mathbf{B}' \mathbf{B}' \rangle \right] \\ + \rho \left[ \frac{GM_\odot}{r^2} \hat{\mathbf{r}} + 2\boldsymbol{\Omega} \times \mathbf{v} + \boldsymbol{\Omega} \times (\boldsymbol{\Omega} \times \mathbf{r}) \right] = 0, \end{aligned} \quad (6)$$

$$\frac{\partial \mathbf{B}}{\partial t} = \nabla \times (\mathbf{v} \times \mathbf{B} + \langle \mathbf{v}' \times \mathbf{B}' \rangle), \quad (7)$$

$$\begin{aligned} \frac{\partial P}{\partial t} + (\mathbf{v} \cdot \nabla) P + \gamma P (\nabla \cdot \mathbf{v}) + \nabla \cdot \langle \mathbf{v}' P' \rangle + (\gamma - 1) \langle P' \nabla \cdot \mathbf{v}' \rangle \\ = -(\gamma - 1) \nabla \cdot \mathbf{q}_H + Q(\mathbf{r}), \end{aligned} \quad (8)$$

where the momentum Equation (2) is now cast in a conservation form (6) and  $\mathbf{I}$  is the identity matrix.

In the Reynolds-averaging approach, the quantities that represent the influence of small-scale fluctuations on the large-scale flow are treated as subgrid-scale entities and their evolution must be described using turbulence models. We need to define the following terms in Equations (5)–(8) that involve turbulent fluctuations: the MHD Reynolds stress tensor  $\mathbf{R} = \langle \rho (\mathbf{v}' \mathbf{v}' - \mathbf{b}' \mathbf{b}') \rangle$ , where  $\mathbf{b}' = \mathbf{B}' / (4\pi \rho)^{1/2}$ , and the fluctuation magnetic pressure  $\langle B'^2 \rangle / 8\pi$  in Equation (6), the mean turbulent electric field  $\langle \mathbf{v}' \times \mathbf{B}' \rangle$  in Equation (7), the flux of mean turbulent pressure  $\langle \mathbf{v}' P' \rangle$ , and the pressure-dilatation term  $(\gamma - 1) \langle P' \nabla \cdot \mathbf{v}' \rangle$  in Equation (8). The relations of these terms with large-scale flow parameters will be discussed in Section 2.3.

### 2.2. Small-scale Equations

Subtracting Equations (6) and (7) from Equations (2) and (3), respectively, and making use of Equation (5), the following evolution equation for the small-scale variables expressed using



the Elsässer variables,  $\mathbf{z}^\pm = \mathbf{v}' \pm \mathbf{b}'$  (Elsasser 1950), can be obtained:

$$\begin{aligned} \frac{\partial \mathbf{z}^\pm}{\partial t} + [(\mathbf{v} \mp \mathbf{V}_A) \cdot \nabla] \mathbf{z}^\pm + \frac{\mathbf{z}^\pm - \mathbf{z}^\mp}{2} \left[ \nabla \cdot \left( \frac{\mathbf{u}}{2} \pm \mathbf{V}_A \right) \right] \\ + (\mathbf{z}^\mp \cdot \nabla)(\mathbf{u} \pm \mathbf{V}_A) \mp \frac{\mathbf{V}_A}{2\rho} (\mathbf{z}^\pm \cdot \nabla)\rho + \frac{1}{\rho} \nabla \bar{P}' \\ + \boldsymbol{\Omega} \times \mathbf{z}^\pm = \mathbf{NL}^\pm + \mathbf{S}^\pm, \end{aligned} \quad (9)$$

where  $\mathbf{V}_A = \mathbf{B}/(4\pi\rho)^{1/2}$  is the Alfvén velocity,  $\mathbf{u} = \mathbf{v} + \boldsymbol{\Omega} \times \mathbf{r}$  is the velocity in the inertial frame of reference,  $\bar{P}'$  is the fluctuation of the sum of thermal and magnetic pressures, and  $\mathbf{NL}^\pm$  and  $\mathbf{S}^\pm$  consolidate local nonlinear and source terms, respectively. Since Equation (9) does not assume  $\nabla \cdot \mathbf{v}' = 0$  (see discussion in Zhou & Matthaeus 1990), it differs slightly from that given by Zhou & Matthaeus (1990) or Breech et al. (2008). In addition, Equation (9) is written in the corotating reference frame, so an extra term due to the Coriolis force appears in Equation (9) (the last term on the left-hand side). Starting from Equation (9) and applying the formalism and assumptions discussed by Breech et al. (2008), a generalized version of the small-scale turbulence transport equations appropriate for super-Alfvénic flow ( $u \gg V_A$ ) can be derived in the form (see Appendix A for details)

$$\frac{\partial Z^2}{\partial t} + (\mathbf{v} \cdot \nabla)Z^2 + \frac{Z^2}{2} \nabla \cdot \mathbf{u} + \sigma_D Z^2 M = -\frac{\alpha f^+(\sigma_c) Z^3}{\lambda} + \dot{E}_{\text{PI}}, \quad (10)$$

$$\begin{aligned} \frac{\partial (Z^2 \sigma_c)}{\partial t} + (\mathbf{v} \cdot \nabla)(Z^2 \sigma_c) + \frac{Z^2 \sigma_c}{2} \nabla \cdot \mathbf{u} - \frac{2\epsilon_m}{\sqrt{4\pi\rho}} \cdot (\nabla \times \mathbf{u}) \\ = -\frac{\alpha f^-(\sigma_c) Z^3}{\lambda}, \end{aligned} \quad (11)$$

$$\frac{\partial \lambda}{\partial t} + (\mathbf{v} \cdot \nabla)\lambda = \beta f^+(\sigma_c) Z - \frac{\beta \lambda \dot{E}_{\text{PI}}}{\alpha Z^2}. \quad (12)$$

Here, the dependent variables are statistical descriptors of the turbulence:  $Z^2 = \langle v'^2 \rangle + \langle b'^2 \rangle$  is twice the incompressible turbulent energy (flow plus magnetic) per unit mass,  $\sigma_c = 2\langle \mathbf{v}' \cdot \mathbf{b}' \rangle / (\langle v'^2 \rangle + \langle b'^2 \rangle)$  is the normalized cross helicity (or Alfvénicity), and  $\lambda$  is the similarity (correlation) length scale.  $\sigma_D = (\langle v'^2 \rangle - \langle b'^2 \rangle) / (\langle v'^2 \rangle + \langle b'^2 \rangle)$  is the normalized energy difference or the residual energy. Following Zhou & Matthaeus (1990), we treat  $\sigma_D$  as a parameter and use its value from observations. Typically,  $\sigma_D$  is observed to be  $\approx -1/3$  (Matthaeus & Goldstein 1982; Tu & Marsch 1995; Yokoi et al. 2008).  $\epsilon_m = -\langle \mathbf{v}' \times \mathbf{B}' \rangle$  is the mean-induced electric field  $\alpha$  and  $\beta$  are the Kármán–Taylor constants of order unity associated with the local phenomenology (Hossain et al. 1995; Matthaeus et al. 1996b).  $f^\pm(\sigma_c) = (1 - \sigma_c^2)^{1/2} [(1 + \sigma_c)^{1/2} \pm (1 - \sigma_c)^{1/2}] / 2$  is the function of cross helicity.  $M$  is a scalar “mixing” term that depends on the type of turbulence symmetry assumed. For transverse to  $\mathbf{B}$  and axisymmetric turbulence  $M = \nabla \cdot \mathbf{u} / 2 - \hat{\mathbf{B}} \cdot (\hat{\mathbf{B}} \cdot \nabla) \mathbf{u}$ , where  $\hat{\mathbf{B}}$  is a unit vector in the direction of magnetic field and for isotropic turbulence  $M = \nabla \cdot \mathbf{u} / 6$ .

$\dot{E}_{\text{PI}}$  is an energy supply rate due to waves originating from newborn interstellar pickup protons. Following Williams et al.

(1995), Isenberg et al. (2003), Smith et al. (2004, 2006), and Breech et al. (2008), we define  $\dot{E}_{\text{PI}}$  as

$$\dot{E}_{\text{PI}} = \frac{f_D u V_A n_H}{n_0 \tau_{\text{ion}}} \exp\left(-\frac{L_{\text{cav}}}{r}\right),$$

where  $f_D$  is a parameter that accounts for the kinetic details of the isotropization process of pickup protons,  $n_H$  is the interstellar hydrogen number density,  $n_0$  is the number density of solar wind protons at 1 AU,  $\tau_{\text{ion}}$  is the neutral ionization time at 1 AU, and  $L_{\text{cav}}$  is the characteristic scale of the ionization cavity around the Sun.

In addition to postulating local incompressibility of fluctuations ( $\rho' = 0$ ), the following assumptions were made in deriving Equations (10)–(12): parameterization of the energy difference tensor by a constant normalized energy difference  $\sigma_D$  (which enters Equation (10) as a free parameter), structural similarity of the correlations (each element of the correlation function tensor is separately proportional to the trace), and single similarity scale  $\lambda$  (which is identified with the correlation scale). For more details on these assumptions, see Breech et al. (2008). The first term on the right-hand side of Equation (11) is the turbulent energy decay that is assumed to go into the internal energy of the solar wind plasma. Consequently, the source of the internal energy in Equation (8) takes the form

$$Q(\mathbf{r}) = \frac{(\gamma - 1)\alpha f^+(\sigma_c)\rho Z^3}{2\lambda}. \quad (13)$$

### 2.3. Modeling the Turbulence Terms

Assuming that turbulence is transverse to the mean magnetic field  $\mathbf{B}$  and axisymmetric about it, the Reynolds stress tensor in Equation (6) takes the form

$$\mathbf{R} = \langle \rho(\mathbf{v}'\mathbf{v}' - \mathbf{b}'\mathbf{b}') \rangle = \frac{\rho}{2}(v'^2 - b'^2)(\mathbf{I} - \hat{\mathbf{B}}\hat{\mathbf{B}}) = \frac{\sigma_D \rho Z^2}{2}(\mathbf{I} - \hat{\mathbf{B}}\hat{\mathbf{B}}),$$

where  $\mathbf{I} - \hat{\mathbf{B}}\hat{\mathbf{B}}$  is a projection tensor into the plane perpendicular to  $\mathbf{B}$ . In the case of an isotropic turbulence, a similar calculation provides  $\mathbf{R} = \sigma_D \rho Z^2 \mathbf{I} / 3$ . Obviously, the mean fluctuating magnetic pressure in Equation (6) can be expressed through the turbulent energy and the energy difference as  $\langle B'^2 \rangle / 8\pi = (1 - \sigma_D)\rho Z^2 / 4$ . As for the mean turbulent electric field, one of the simplest options is to assume  $\epsilon_m = \hat{\alpha} Z \mathbf{B}$ , where  $\hat{\alpha}$  is the dynamo parameter of order unity (Matthaeus et al. 1986). The flux of the mean turbulent ram pressure,  $\langle \mathbf{v}' P' \rangle$ , and the dilatation term  $(\gamma - 1)\langle P' \nabla \cdot \mathbf{v}' \rangle$  in Equation (8) will be just neglected in the present work, as we shall treat the local turbulence as incompressible.

We recall briefly that there are numerous indications that fluctuations in the solar wind are mainly of the incompressible variety. The fluctuations are observed to be transverse, quasi two dimensional, and “Alfvénic” (Belcher & Davis 1971; Matthaeus et al. 1990), each of which is suggestive of low compressional activity. Furthermore, from a theoretical perspective, magnetosonic modes are strongly damped for solar wind parameters (Barnes 1979). Under such circumstances, it is possible to understand that turbulence in a compressible medium can evolve in a nearly incompressible fashion and such a description is consistent with numerous observational features (Zank & Matthaeus 1992). Although a refined description would take compressional fluctuations into account (e.g., Yoshizawa 1992), these observations and theoretical ideas amply motivate the use of local incompressibility as a useful approximate description of solar

wind turbulence at scales smaller than the turbulence outer scale (typically  $< 0.01$  AU near Earth orbit).

#### 2.4. The Governing System of Equations

The combined system of large- and small-scale equations (5)–(12) can be re-written in a quasi-conservation form as

$$\frac{\partial \mathbf{W}}{\partial t} + \nabla \cdot \mathbf{F} = \mathbf{S}, \quad (14)$$

where  $\mathbf{W} = (\rho, \rho \mathbf{u}, \mathbf{B}, E, Z^2, Z^2 \sigma_c, \rho \lambda)^T$ ,

$$\mathbf{F} = \begin{pmatrix} \rho \mathbf{v} \\ \rho \mathbf{v} \mathbf{u} - \frac{\eta}{4\pi} \mathbf{B} \mathbf{B} + \bar{P} \mathbf{I} \\ \mathbf{v} \mathbf{B} - \mathbf{B} \mathbf{v} \\ \mathbf{v} E + \mathbf{u} \bar{P} - \frac{\eta \mathbf{B}(\mathbf{u} \cdot \mathbf{B})}{4\pi} + \mathbf{q}_H \\ Z^2 \mathbf{v} \\ Z^2 \sigma_c \mathbf{v} \\ \rho \lambda \mathbf{v} \end{pmatrix},$$

$$\mathbf{S} = \begin{pmatrix} 0 \\ -\rho \left( \frac{GM_\odot}{r^2} \hat{\mathbf{r}} + \boldsymbol{\Omega} \times \mathbf{u} \right) \\ -\nabla \times \boldsymbol{\epsilon}_m \\ -\rho \mathbf{V}_A \cdot (\nabla \times \boldsymbol{\epsilon}_m) + \frac{\rho \dot{E}_{PI}}{2} \\ Z^2 \left[ \frac{\nabla \cdot \mathbf{u}}{2} - \sigma_D M - \frac{\alpha f^+(\sigma_c) Z}{\lambda} \right] + \dot{E}_{PI} \\ \frac{Z^2 \sigma_c}{2} \nabla \cdot \mathbf{u} + \frac{2\boldsymbol{\epsilon}_m \cdot (\nabla \times \mathbf{u})}{\sqrt{4\pi\rho}} - \frac{\alpha f^-(\sigma_c) Z^3}{\lambda} \\ \rho \beta \left[ f^+(\sigma_c) Z - \frac{\lambda \dot{E}_{PI}}{\alpha Z^2} \right] \end{pmatrix},$$

where  $E$  is the total energy density that involves kinetic, thermal, magnetic, gravitational, and turbulent components

$$E = \frac{\rho u^2}{2} + \frac{P}{\gamma - 1} + \frac{B^2}{8\pi} - \frac{\rho GM_\odot}{r} + \frac{\rho Z^2}{2},$$

and  $\bar{P} = P + B^2/8\pi + P_w$  is the total pressure, including the turbulent pressure  $P_w$ . In the case of transverse and axisymmetric turbulence,  $P_w = (\sigma_D + 1)\rho Z^2/4$  and  $\eta = 1 + 2\pi\sigma_D\rho Z^2/B^2$ , and for isotropic turbulence  $P_w = (\sigma_D + 3)\rho Z^2/12$  and  $\eta = 1$ . The derivation of the momentum and total energy equations in Equation (14) is given in Appendix B.

#### 2.5. Hollweg's Heat Flux

Within the solar wind, the electron heat flux is directed primarily along the magnetic field. In the inner corona ( $r \leq 5$ – $10 R_\odot$ ,  $R_\odot$  is the radius of the Sun), where the collisions between particles are relatively frequent, the heat flux can be approximated by the classical collision-dominated model of Spitzer & Härm (1953). Beyond the inner corona, the plasma is virtually collisionless and the electron heat flux is dominated by a non-local suprathermal tail of electron distribution (Scudder & Olbert 1979). Because a collision-dominated model is not applicable in this case, Hollweg (1974, 1976) proposed a “collisionless” approximation

$$\mathbf{q}_H = \frac{3}{2} a P_e \mathbf{v}, \quad (15)$$

where  $a$  is a parameter of order unity. The formula (15) was later recovered by Canullo et al. (1996) from their solution of the Fokker–Planck equation in the limit  $r \geq 6 R_\odot$  for suprathermal electrons originating near the solar corona base. It was also demonstrated recently by Cranmer et al. (2009) that Hollweg's approximation (15) with  $a = 1.05$  matches closely *Helios* observations from 0.3–1 AU (Pilipp et al. 1990) and *Ulysses* observations beyond 1 AU (Scime et al. 1999). In this paper, we describe the electron heat flux explicitly by incorporating Hollweg's expression (15) into the energy equation (8).

Because our approach is one fluid and assumes that the pressures (and temperatures) of protons and electrons are equal,  $P_e = P_p = P/2$ , Equation (15) takes the form  $\mathbf{q}_H = (3/4)a P \mathbf{v}$ . Note that in steady-state case, applying this expression is mathematically identical to assuming a polytropic law, with the polytropic index  $\gamma$  that depends on  $a$  as  $\gamma = (5 + \frac{3}{2}a)/(3 + \frac{3}{2}a)$  (Jacques 1978; Meyer-Vernet 2007). It is interesting that according to this formula, the empirical value  $a = 1.05$  of Cranmer et al. (2009) corresponds closely to  $\gamma = 1.46$  inferred by Totten et al. (1995) from *Helios* proton data, which means that in one-fluid solar wind models, using Totten et al.'s empirical index is almost equivalent to employing Hollweg's heat flux.

#### 2.6. Numerical Approach, Initial, and Boundary Conditions

In the context of the present study, we are interested in steady-state solutions of the time-dependent system (14). For this purpose, we apply a time-relaxation method, i.e., integration of the governing equations in time until a steady state is reached. To integrate Equation (14) numerically in time, we use the Central Weighted Essentially Non-Oscillatory (CWENO) scheme of Kurganov & Levy (2000) with a global smoothness indicator (Levy et al. 1999). The CWENO scheme is a spatially third-order, semi-discrete method that applies a piecewise polynomial reconstruction and smoothness indicators. In smooth regions, the polynomial reconstruction guarantees the maximum order of accuracy, but in the presence of a discontinuity it automatically switches to the best one-sided stencil, which generates the least oscillatory reconstruction. For the time evolution, the strong stability-preserving (SSP) Runge–Kutta discretization (Gottlieb et al. 2001) of third order has been implemented. To maintain the  $\nabla \cdot \mathbf{B} = 0$  constraint, the relaxation code implements the eight-wave scheme of Powell (1994) that requires adding source terms of the form  $-\mathbf{B}(\nabla \cdot \mathbf{B})/4\pi$ ,  $-\mathbf{v}(\nabla \cdot \mathbf{B})$ , and  $-(\mathbf{B} \cdot \mathbf{u})(\nabla \cdot \mathbf{B})/4\pi$  into the right-hand side of the momentum, induction, and total energy equations, respectively.

Equations (10)–(12) are valid only assuming that  $u \gg V_A$  and therefore following the approach of Breech et al. (2008), we have chosen to place our inner boundary far enough from the Sun at 0.3 AU where the solar wind flow is already highly super-Alfvénic. To specify the dependent variables at the boundary and throughout the computational region in the initial state, we use the output from the model of Usmanov & Goldstein (2003), which is based on solving the MHD equations for a single-fluid polytropic flow driven by thermal and WKB Alfvén wave pressure gradients. The density, velocity, magnetic field, and thermal pressure at the inner boundary are directly taken from a solution of Usmanov & Goldstein (2003) for a source dipole field on the Sun aligned with the solar rotation axis.  $Z^2$  is calculated from the WKB Alfvén wave energy density  $\mathcal{E}$  (see Usmanov & Goldstein 2003) as  $Z^2 = 2\mathcal{E}/\rho$  on the boundary, and  $Z^2$  is set to be independent of  $\theta$  and to decrease as  $r^{-2}$  throughout the rest of the domain in the initial state. The boundary conditions for  $\lambda$  and  $\sigma_c$  are specified similarly to those

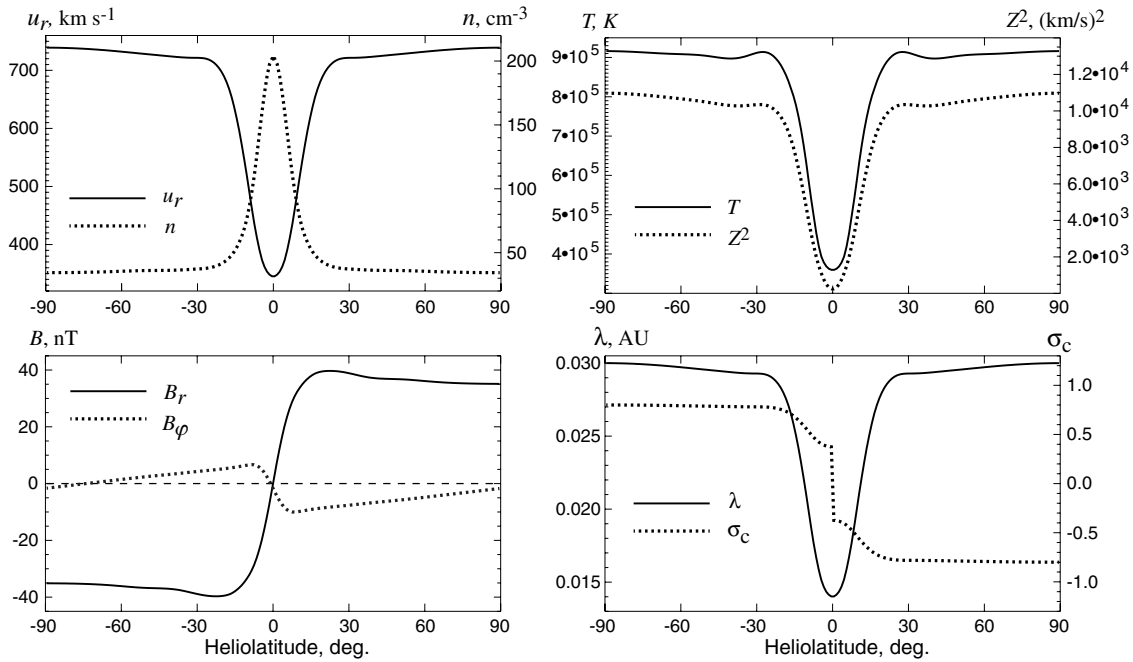


**Figure 1.** Boundary profiles of plasma/magnetic field and turbulence variables at 0.3 AU as a function of heliolatitude.

used by Breech et al. (2008):  $\lambda$  is set to vary from 0.03 AU in the fast wind to 0.015 AU in the slow one, while  $\sigma_c$  is  $\pm 0.8$  in the fast wind (plus or minus depending on the sign of the radial magnetic field) and changing sign on the equator. Figure 1 illustrates the boundary conditions prescribed at 0.3 AU.

The convenience of solving the governing equations (14) in the rotating reference frame is that the boundary values are simply fixed in time. It is worth noting that the momentum and energy equations included in Equation (14) were transformed from Equations (5)–(8) using the substitution  $\mathbf{v} = \mathbf{u} - \boldsymbol{\Omega} \times \mathbf{r}$  that notably simplifies the equations (see Appendix B for details) and permits one to advance in time the inertial momentum  $\rho \mathbf{u}$  (instead of the linearly increasing rotating frame momentum  $\rho \mathbf{v}$ ) and the inertial total energy  $E$ .

The numerical code that we have developed for integrating Equation (14) is fully three-dimensional and it uses a composite grid of spherical coordinates that consists of a main spherical grid and two “patches” covering the norther and souther polar caps and partially overlapping with the main grid (Usmanov 1996; Usmanov & Goldstein 2003). The main grid encompasses all longitudes within a latitude range (extending to  $67^\circ 5'$  of latitude) that is not significantly affected by the spherical coordinate singularity near the poles. The composite grid approach has been developed to circumvent the specific difficulty of the geometrical singularity on the pole axis and the condensing of grid points in spherical coordinates toward the poles.

In the present study, we apply the code for an axisymmetric problem in the spherical shell extending from 0.3 to 100 AU. There are 300 grid points in the radial direction with a logarithmic increase of the spacing from 0.06 AU to  $\sim 1.8$  AU at the outer boundary. The latitudinal grid resolution is  $1^\circ$ . The model includes a number of parameters that were taken as follows:  $\gamma = 5/3$ , Hollweg’s parameter  $a = 1$ , the Kármán–Taylor constants  $\alpha = 2\beta = 0.8$  (Smith et al. 2006), the normalized energy difference  $\sigma_D = -1/3$ , the isotropization parameter  $f_D = 0.25$ , the interstellar neutral hydrogen density  $n_H = 0.1 \text{ cm}^{-3}$ , the neutral ionization time at 1 AU  $\tau_{\text{ion}} = 10^6 \text{ s}$ , and the scale of the ionization cavity around the Sun  $L_{\text{cav}} = 8 \text{ AU}$ . Most of the

parameters listed above are the same as in Breech et al. (2008). Also, in what follows we neglect the turbulent electric field ( $\hat{\alpha} = 0$ ). Furthermore, we restrict our attention to turbulence having its vector components perpendicular to the mean magnetic field. Such turbulence is sometimes called “transverse” or “Alfvén mode” (Belcher & Davis 1971; Goldreich & Sridhar 1995) in view of its apparent correspondence to wave theory (Barnes 1979). However, transverse turbulence also emerges in nearly incompressible turbulence theory and simulations (Zank & Matthaeus 1992; Matthaeus et al. 1996a) and is a central element of weak turbulence (Galtier et al. 2000).

The outer boundary conditions at 100 AU were chosen to be of open type, which is usually approximated by a first-order (linear) extrapolation.

### 3. SIMULATION RESULTS AND ANALYSIS

Starting from the initial distribution of plasma, magnetic field, and turbulence parameters at time  $t = 0$ , the system is allowed to relax for 12,000 hr or  $\sim 1.4$  yr. Because the initial state is merely a superposition of the solution from Usmanov & Goldstein (2003; for  $\rho$ ,  $\mathbf{u}$ ,  $\mathbf{B}$ , and  $P$ ) on the one hand, and of some initial distribution of the turbulence parameters ( $Z^2$ ,  $\sigma_c$ , and  $\lambda$ ) on the other, the system evolves in time toward a state in which all forces are balanced. In the supersonic and super-Alfvénic flow that we deal with, all disturbances propagating in any direction are convected outward, so the relaxation time is essentially the time for the slowest plasma parcel to traverse the computational domain in the radial direction. When the transient is exiting the domain, the linear extrapolation that we use for assigning boundary conditions on the outer boundary can, at times, produce negative values of density. Should that happen, the linear extrapolation is temporarily switched over to a zero-order extrapolation.

An example of the “relaxation transient” is shown in Figure 2. The transient forms in the initially ( $t = 0$  hr) latitude-independent distribution of  $Z^2$  (although  $Z^2$  varies with latitude on the inner boundary; see Figure 1), it propagates outward and leaves behind a steady-state structure with maximum values of

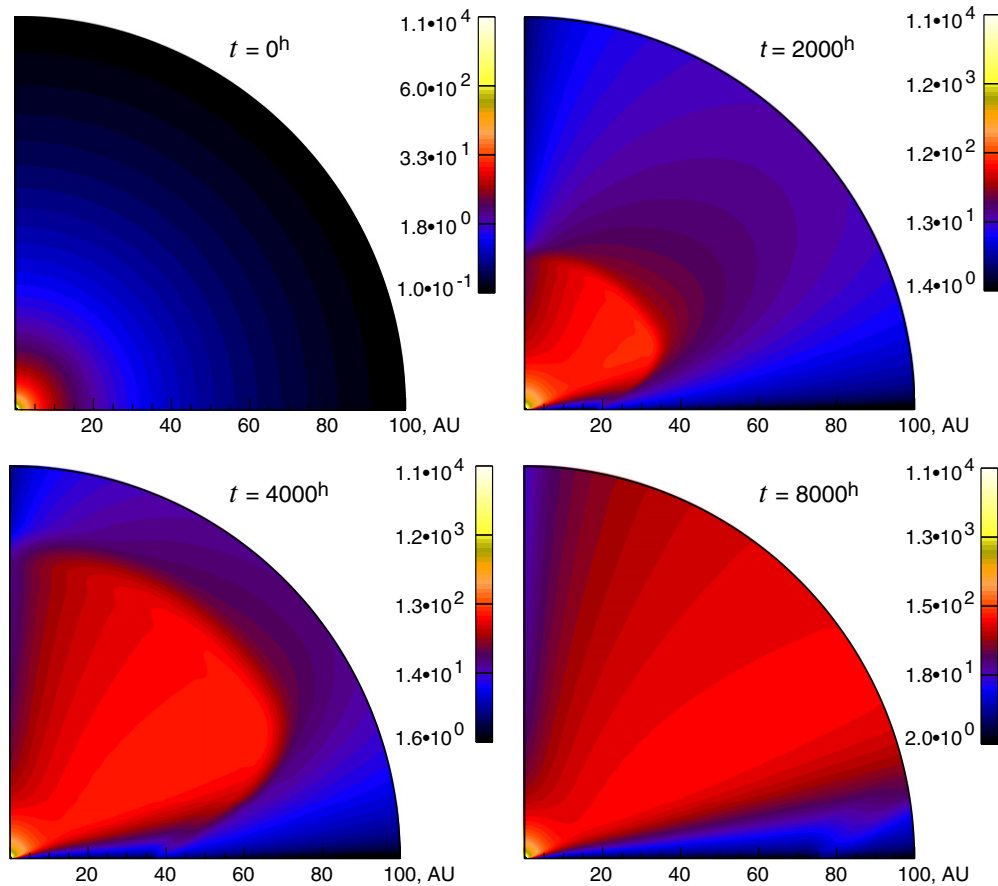


**Figure 2.** Relaxation of the initially ( $t = 0$ ) latitude-independent distribution of  $Z^2$  ( $\text{km}^2 \text{s}^{-2}$ ) in the meridional plane between the pole (vertical edge) and the equator (horizontal edge). Contour maps are shown for  $t = 0, 2000, 4000$ , and  $8000$  hr.

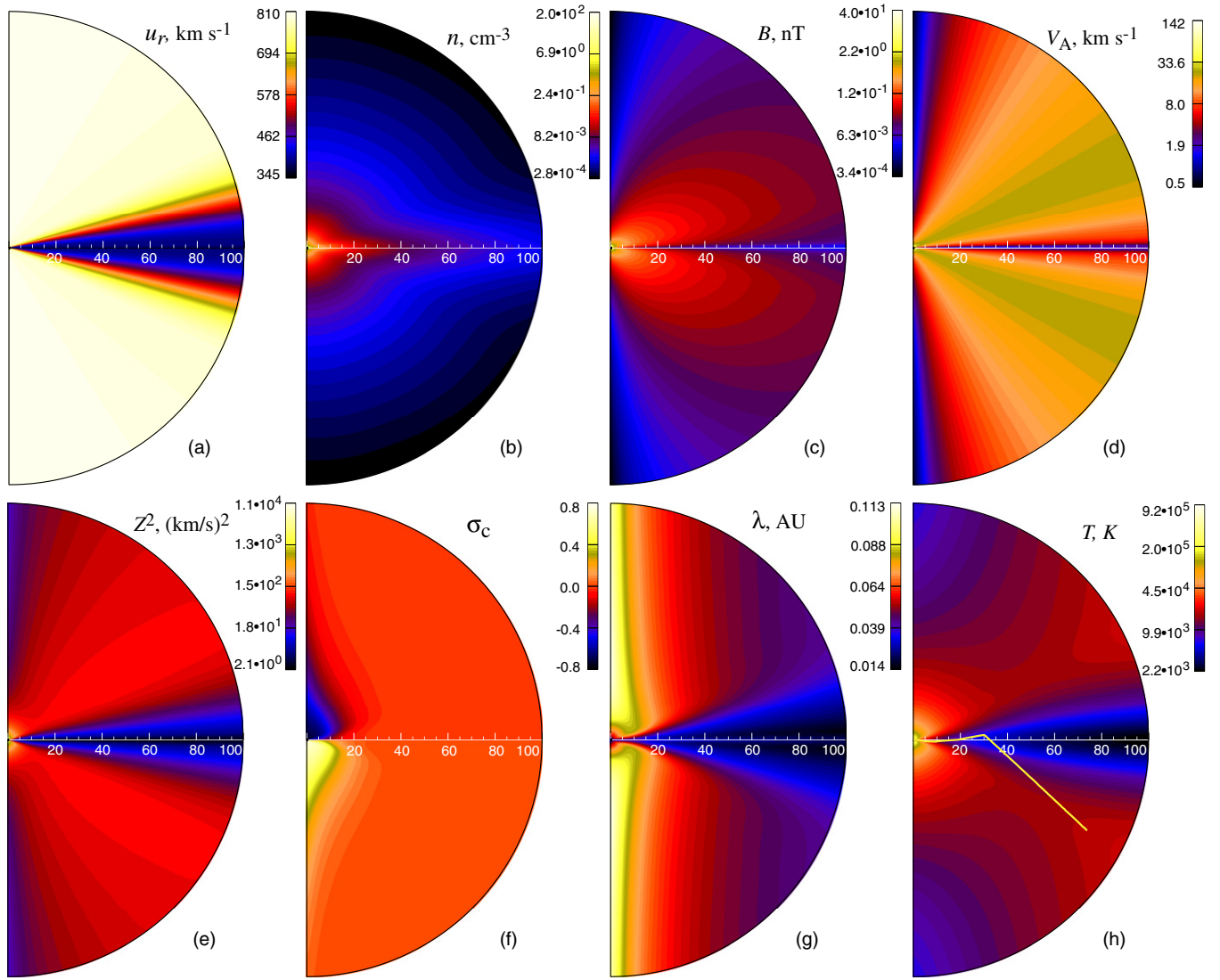
$Z^2$  at  $\sim 30^\circ$  of heliolatitude. At  $t = 8000$  hr, the relaxation is complete at all latitudes except for the slow wind region near the equator.

Figure 3 presents the result of relaxation at  $t = 12,000$  hr. The solar wind structure is typical for solar cycle minimum: a band of slow wind near the equator and a fast ( $\sim 800 \text{ km s}^{-1}$ ) and relatively uniform wind at higher latitudes. The lowest speed at the inner boundary is  $\sim 370 \text{ km s}^{-1}$ , so neglecting the (insignificant) solar wind acceleration beyond 0.3 AU it takes  $\sim 1.3$  years for a “relaxation” transient to propagate through and to leave the computational domain at 100 AU. The magnetic field magnitude  $B$  is relatively small on the polar axis where the azimuthal magnetic component  $B_\phi = 0$  and  $B = 0$  on the helioequator that separates inward and outward magnetic field sectors ( $B_r = 0$  and therefore  $B_\phi = 0$ ). As a result,  $B$  has a maximum at latitudes of  $\sim 15^\circ$ , which along with the latitudinal profile of  $n$  translates into variations of the pickup-proton driving term,  $\dot{E}_{\text{PI}}$ , and the turbulence energy,  $Z^2$ , with a maximum at  $\sim 30^\circ$ . The distribution of Alfvén speed depends on latitude in a similar way, but it is essentially independent of heliocentric distance beyond  $\sim 10$  AU. The plasma temperature  $T$  is relatively low near the helioequator and reaches a maximum at  $\sim 30^\circ$  as well. The heating effect of pickup protons is obvious from the  $T$  plot: the temperature increases with the heliocentric distance beyond  $\sim 30$  AU except near the pole and the equator. The variations of  $T$ ,  $Z^2$ ,  $\lambda$ , and  $\sigma_c$  are generally similar to the results of Breech et al. (2008; cf. with their Figures 8, 10, 12, and 14, respectively). In particular, both models show higher levels of turbulence around the transition between slow and fast

solar wind, while turbulence is depressed both over the poles and in slow wind near the equator, where the turbulence drivers, especially stream shear, are small. The details of the distributions are however noticeably different between the two models. For example, the results shown in Figure 3 are smoother than the analogous results of Breech et al. (2008) due to the latitudinal effects that the present model describes self-consistently. Also shown in Figure 3(h) is the projection of *Voyager 2* trajectory on the meridional plane. The excursion of the spacecraft into the southern hemisphere began at  $\sim 30$  AU after its encounter with Neptune in 1989.

Figure 4 demonstrates the radial variations of the flow and turbulence parameters for heliolatitudes spaced by  $30^\circ$  from the pole to the equator.  $B$  is zero on the equator because in our axisymmetric model, it coincides with the current sheet where all components of  $\mathbf{B}$  are equal to zero. On the pole,  $B$  is determined by the radial component  $B_r$  that varies with radius as  $r^{-2}$ , while at lower latitudes the main contribution is from the azimuthal component  $B_\phi \sim r^{-1}$ . The plot for  $u_r$  illustrates again the uniformity of fast solar wind as evidenced by the slight difference between the radial curves at  $30^\circ$ ,  $60^\circ$ , and  $90^\circ$ . After a steep fall inside 1 AU, the Alfvén speed  $V_A$  shows little dependence on radius beyond  $\sim 10$  AU. (Note that  $V_A = 0$  on the equator in our case.) At higher latitudes, the flattening appears at smaller distances. The plasma density  $n$  decreases with distance as  $r^{-2}$  at all latitudes. The temperature profiles at various latitudes in fast wind are indistinguishable below 20 AU, but the rise beyond 20 AU differs as a function of latitude as determined by the latitudinal dependence of the driving term





**Figure 3.** Contour plots in the meridional plane from 0.3 to 100 AU of the following model variables: the radial velocity  $u_r$ , number density  $n$ , magnetic field magnitude  $B$ , Alfvén velocity  $V_A$ , turbulent energy  $Z^2$ , cross helicity  $\sigma_c$ , correlation length scale  $\lambda$ , and plasma temperature  $T$ . The yellow line in the  $T$  plot depicts the projection of the *Voyager 2* trajectory on the meridional plane.

$\dot{E}_{PI}$ , which causes slight increases in thermal pressure that can also be seen in the plot of  $P$ . In fast wind, the turbulence energy  $Z^2$  is not dependent on latitude up to  $\sim 10$  AU, while the profiles of the cross helicity  $\sigma_c$  and of the similarity scale  $\lambda$  become different at  $\sim 5$  AU. The value of  $Z^2$  on the equator is more than an order of magnitude smaller than it is in fast wind, due to both variations in the inner boundary, which has small values near the equator and also due to the smaller driving effect of pickup protons. In fast wind,  $\sigma_c$  changes slowly from  $-0.8$  to  $-0.6$  up to  $\sim 5$  AU and then the curves diverge abruptly with larger decreases at lower latitudes. (Note that  $\sigma_c = 0$  on the equator in our case.) The radial variations of  $\lambda$  show a maximum that moves to larger distances at higher latitudes. The maximum is a result of the interplay between the first and second terms in the right-hand side of Equation (12).

Comparisons between the one-dimensional model results of Breech et al. (2008) and the present model are shown in Figure 5. The solutions of Breech et al. (2008) use the same boundary values at 0.3 AU shown in Figure 1. The comparisons are presented for a high latitude ( $\theta = 15^\circ$ ) and demonstrate two sets of plots: one comparing against normal Breech et al.’s

parameters, including a free parameter of the strength of shear driving  $C_{sh} = 0.5$  and, second, with  $C_{sh}$  dropped to 0.20. The solutions for  $Z^2$  and  $T$  look comparable in both cases. The solutions for  $\lambda$  and  $\sigma_c$  demonstrate better agreement for the lower value of  $C_{sh}$ .  $C_{sh}$  is introduced into the constant-velocity model of Breech et al. (2008) as a measure of the turbulence driving due to a presumptive instability of large-scale sheared flows that generates additional small-scale turbulence energy. The present model does not appear to require such a parameter because sheared flows are explicitly present in the solution, but, as follows from the comparison, the shear driving is generally weaker than in the typical one-dimensional solution of Breech et al. (2008). This contrast may be due to terms that are absent in the Reynolds decomposition approach. We discuss this further in the summary section.

Figure 6 shows comparison of the model results presented in Figure 3 with *Ulysses* data collected during *Ulysses*’ first fast latitude scan in 1994–1995 for latitudes from  $-80.2$  to  $+80.2$  and for the range of heliocentric distances from 1.3 to 2.3 AU. As is evident from Figure 6, there is rough agreement between the computed and observed curves in each plot. Both latitude

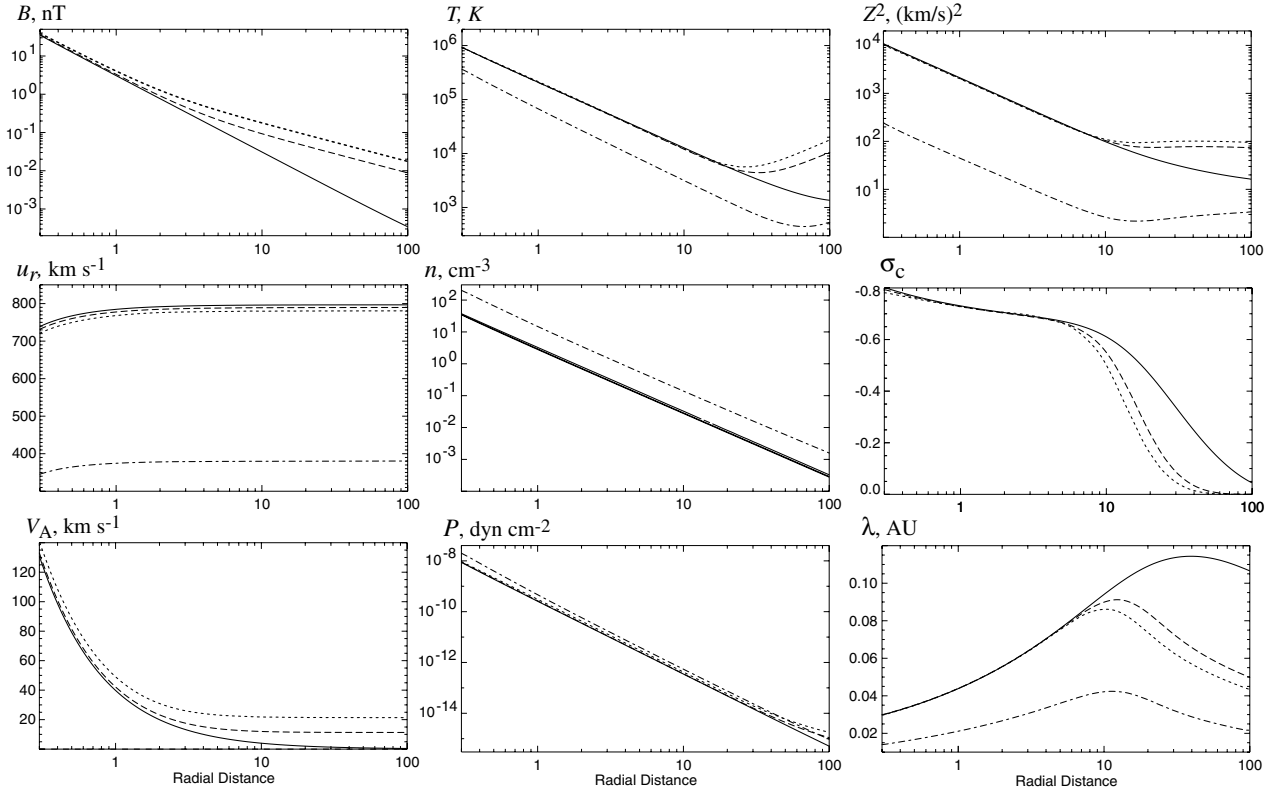


**Figure 4.** Radial profiles of the flow, magnetic field, and turbulence quantities at heliolatitudes of  $90^\circ$  (the pole, solid lines),  $60^\circ$  (dashed lines),  $30^\circ$  (dotted lines), and  $0^\circ$  (the equator, dash-dotted lines).

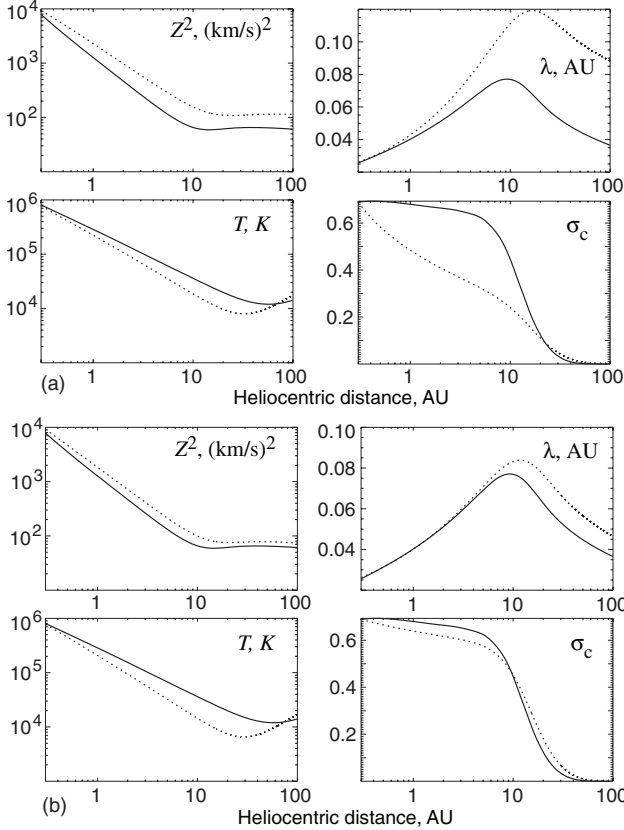


**Figure 5.** Comparison of the present model with the one-dimensional model of Breech et al. (2008) at  $\theta = 15.5^\circ$ . Solid line is the present code and the dotted line is the model of Breech et al. (2008) for  $C_{SH} = 0.5$  (a) and  $C_{SH}$  dropped to 0.20 (b).

and intensity variations of the computed quantities are similar to those in the *Ulysses* data. The bimodal structure of the solar wind with the relatively uniform and tenuous fast wind is fairly well reproduced by the model.

Figure 7 shows radial variations of the computed temperature along the trajectory of *Voyager 2* with the proton temperature observed by *Voyager 2*. To produce this comparison, the model structure was artificially tilted by  $10^\circ$  with regard to the solar rotation axis, to account for the tilt typical around solar minima. There is generally good agreement between the model and *Voyager 2* observations with the evident inflection point at  $\sim 35$  AU. The important factor that influences the temperature profile is the southward displacement of *Voyager 2* (Figure 7(c)) outside 30 AU. Figure 7(a) shows an additional model profile computed along the projection of the *Voyager* trajectory on the helioequatorial plane. The deviation of the model curves along the *Voyager 2* trajectory and along its equatorial projection gives an estimate of the latitudinal effect in the *Voyager 2* observations. Another essential aspect of the comparison is that the *Voyager* observations cover the period of 30 years, or almost three solar cycles (Figure 7), so that the present model constructed for solar minimum conditions is a very rough approximation.

The temperature profiles computed without Hollweg's heat flux ( $\mathbf{q}_H = 0$ ), without any turbulence effects ( $Z^2 = 0$ ), for zero tilt, and without pickup proton effects ( $\dot{E}_{PI} = 0$ ) are shown in Figure 7(b). Comparison of the solutions demonstrates that, in the present model, the major heating effect is associated with the heat flux. The effect of the turbulent cascade is relatively small in comparison with the heating by pickup protons.

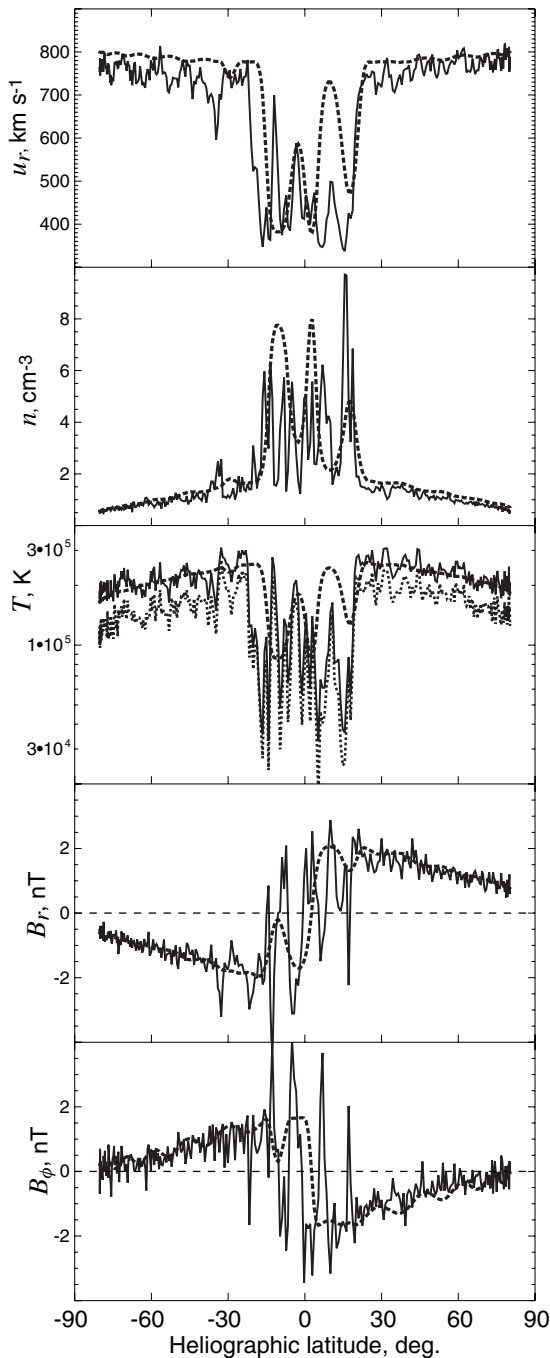


**Figure 6.** Variations of model parameters (dashed lines) computed along the *Ulysses* trajectory during its first fast latitude scan from 1994 September 13 to 1995 July 13. The solid lines represent daily averages of *Ulysses* plasma and magnetic field data. There are two estimates of the proton temperature measured by *Ulysses*: “T-large”/“T-small” shown by the solid/dotted line.

#### 4. SUMMARY

We have presented the first results of a novel approach to modeling the super-Alfvénic solar wind together with the distribution of turbulence throughout the heliosphere. The mass, momentum, induction, and energy equations for the large-scale solar wind flow have been solved simultaneously with the transport equations for turbulence energy, normalized cross helicity, and correlation scale. The model was applied to simulate the self-consistent interaction between the large-scale solar wind and smaller-scale turbulence. The two-scale approach

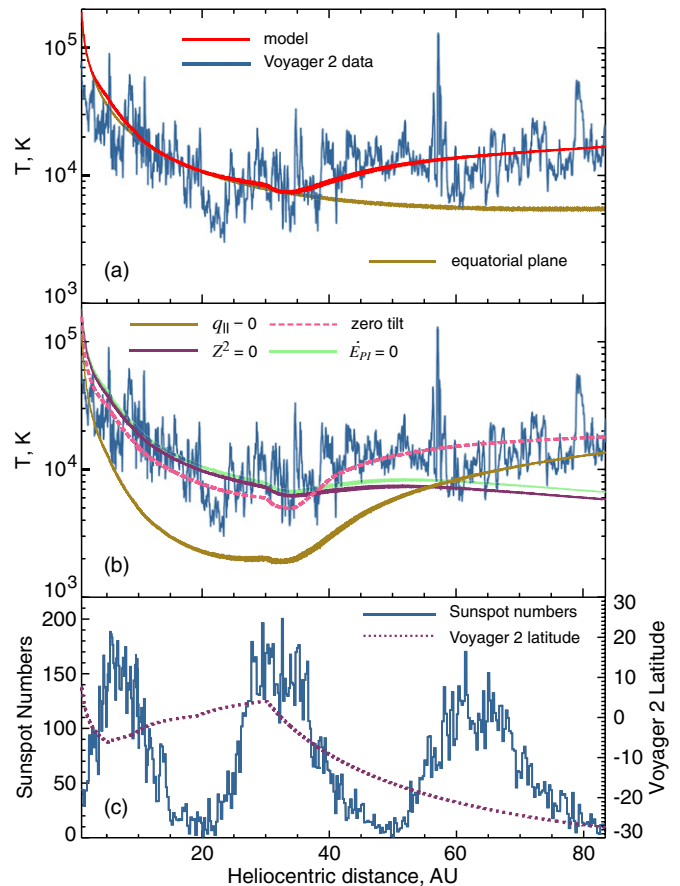


**Figure 7.** Radial variations of the model temperature (27 day running averages) computed along the trajectory of *Voyager 2* and along its pseudo-trajectory assuming that the spacecraft remained in the helioequatorial plane superimposed on 27 day running averages of *Voyager 2* proton temperature data from 1977 to 2007 (a). The model temperatures computed without the electron heat flux ( $q_{||} = 0$ ), with no turbulence effects ( $Z^2 = 0$ ), with zero tilt, and without the effect of pickup protons ( $\dot{E}_{p1} = 0$ ) are shown in (b). The bottom panel (c) shows the monthly sunspot numbers and heliographic latitude of *Voyager 2*. Note that the  $10^\circ$  tilted dipole model is appropriate only for periods of low solar activity.

was used to study the effects of turbulence dissipation and pickup-proton-associated heating on the plasma temperature. We have also compared the simulation results with *Ulysses* and *Voyager 2* observations and have shown that the model agrees with the *Ulysses* data and follows the *Voyager 2* observed temperature evolution fairly well despite the fact that the model is best suited for solar minimum conditions.

It should be noted that the amount of turbulent heating in the model of Breech et al. (2008) differs from the present model by a factor of two. The difference arises from the one-fluid formalism of the present model that assumes that the cascading energy gets split between electrons and protons instead of feeding only protons as in Breech et al. (2008). In this respect, the present one-fluid model seems to be similar to the two-fluid model of Breech et al. (2009) in which the cascading energy is also split between protons and electrons, and thus the protons receive much less heating (60%) than in the Breech et al. (2008) model. It is easy to show that the two-fluid formulation of Breech et al. (2009) is reduced to the present formulation of the energy equation if the temperatures of protons and electrons are assumed to be equal.

The model presented in this paper can be applied to the problems of solar modulation of galactic cosmic rays and propagation of solar energetic particles (SEPs). The computed large-scale plasma/magnetic field parameters and turbulence

quantities are precisely what is needed for a realistic study of the propagation of energetic particles in the heliosphere. These are natural applications in that scattering of energetic charged particles depends upon details of the large-scale heliospheric fields as well as on the spatial distribution of the turbulence. For this reason, we suggest that it is important to further develop models such as the present one, as this model self-consistently provides both of these classes of information.

As the next major step with the present model, we plan on extending it to fully three-dimensional case to perform simulations with the source dipole on the Sun tilted with respect to the solar rotation axis. Other planned developments include turning on and studying effects of a turbulent electric field, allowing the fluctuations to be compressible by relaxing the assumption that  $\rho' = 0$ , and including pickup protons as a separate fluid (with a separate mass and energy equation, following the approach of Usmanov & Goldstein 2006). Another development of the model will be to generalize the turbulence transport equations and boundary conditions to make them appropriate for studying sub-Alfvénic solar wind. Such an extension will extend the model by placing the inner boundary at the coronal base.

Finally, we recall that the present straightforward Reynolds-averaged scheme does not include large-scale couplings that drain energy from large scales and directly excite small-scale modes. In this sense, the Reynolds-averaged approach is not complete for cases in which, for example, large-scale convection  $(\mathbf{u} \cdot \nabla)\mathbf{u}$  directly drives small-scale fluctuations. Such a “direct supply” term replenishes turbulence and is typically employed in hydrodynamics LES schemes (see e.g., Germano et al. 1991; Lesieur et al. 2005). We are currently studying extensions to the present model that would take into account this direct supply of small-scale turbulence by non-equilibrium large-scale MHD fields.

We acknowledge the use of *Ulysses* and *Voyager 2* data supplied by the National Space Science Data Center. The work of A.V.U. was supported by NASA grants NNG06GE65G and NNX09AH79G to the University of Delaware. W.H.M. was partially supported by the NASA Heliophysics Theory Program NNX08A147G and by the NSF Solar Terrestrial Program ATM-0539995. B.A.B.’s research was supported by an appointment to the NASA Postdoctoral Program at Goddard Space Flight Center. Resources supporting this work were provided by the NASA High-End Computing (HEC) Program through the NASA Advanced Supercomputing (NAS) Division at the Ames Research Center and the NASA Center for Computational Sciences (NCCS) at the Goddard Space Flight Center.

## APPENDIX A

### SMALL-SCALE EQUATIONS FOR $Z^2$ AND $Z^2\sigma_c$

The derivation follows the procedure and assumptions described in details by Breech et al. (2008). The first step is to form the correlation functions

$$R_{ij}^{\pm}(\mathbf{r}, \boldsymbol{\zeta}) = \langle z_i^{\pm}(\mathbf{r}) z_j^{\pm}(\mathbf{r} + \boldsymbol{\zeta}) \rangle = \langle z_i^{\pm} z_j^{\pm*} \rangle, \quad (\text{A1})$$

where  $\langle \dots \rangle$  is the Reynolds-averaging operator and the star superscript denotes the displaced position  $\mathbf{r} + \boldsymbol{\zeta}$ . By writing Equation (9) in component form for  $z_i^{\pm}$  and  $z_j^{\pm*}$ , multiplying (on the left) the two-component equations by  $z_j^{\pm*}$  and  $z_i^{\pm}$ ,

respectively, and then adding the resultant equations, we have

$$\begin{aligned} & \frac{\partial}{\partial t} (z_i^{\pm} z_j^{\pm*}) + [(\mathbf{v} \mp \mathbf{V}_A) \cdot \nabla] (z_i^{\pm} z_j^{\pm*}) + \frac{2z_i^{\pm} z_j^{\pm*} - z_i^{\pm} z_j^{\mp*} - z_i^{\mp} z_j^{\pm*}}{2} \\ & \times \left[ \nabla \cdot \left( \frac{\mathbf{u}}{2} \pm \mathbf{V}_A \right) \right] + (z_j^{\pm*} z_k^{\mp}) \frac{\partial(u_i \pm V_{Ai})}{\partial r_k} \\ & + (z_i^{\pm} z_k^{\mp*}) \frac{\partial(u_j \pm V_{Aj})}{\partial r_k} \mp \frac{V_{Ai} z_j^{\pm*}}{2\rho} z_k^{\pm} \frac{\partial \rho}{\partial r_k} \mp \frac{V_{Aj} z_i^{\pm}}{2\rho} z_k^{\pm*} \frac{\partial \rho}{\partial r_k} \\ & + \frac{1}{\rho} (z_j^{\pm*} \nabla_i \bar{P}' + z_i^{\pm} \nabla_j \bar{P}') + z_j^{\pm*} (\boldsymbol{\Omega} \times \mathbf{z}^{\pm})_i + z_i^{\pm} (\boldsymbol{\Omega} \times \mathbf{z}^{\pm*})_j \\ & = z_j^{\pm*} (N L_i^{\pm} + S_i^{\pm}) + z_i^{\pm} (N L_j^{\pm} + S_j^{\pm}). \end{aligned} \quad (\text{A2})$$

Applying the Reynolds averaging to Equation (A2) leads to the equation for the correlation functions

$$\begin{aligned} & \frac{\partial R_{ij}^{\pm}}{\partial t} + [(\mathbf{v} \mp \mathbf{V}_A) \cdot \nabla] R_{ij}^{\pm} + R_{ij}^{\pm} \left[ \nabla \cdot \left( \frac{\mathbf{u}}{2} \pm \mathbf{V}_A \right) \right] \\ & + \Pi_{ij}^{\pm} = N L_{ij}^{\pm} + S_{ij}^{\pm}, \end{aligned} \quad (\text{A3})$$

where  $\Pi_{ij}^{\pm}$  is the mixing tensor

$$\begin{aligned} \Pi_{ij}^{\pm} = & - \frac{\langle z_i^{\pm} z_j^{\mp*} \rangle + \langle z_i^{\mp} z_j^{\pm*} \rangle}{2} \left[ \nabla \cdot \left( \frac{\mathbf{u}}{2} \pm \mathbf{V}_A \right) \right] \\ & + \langle z_j^{\pm*} z_k^{\mp} \rangle \frac{\partial(u_i \pm V_{Ai})}{\partial r_k} + \langle z_i^{\pm} z_k^{\mp*} \rangle \frac{\partial(u_j \pm V_{Aj})}{\partial r_k} \\ & \mp \frac{V_{Ai}}{2\rho} \langle z_k^{\pm} z_j^{\pm*} \rangle \frac{\partial \rho}{\partial r_k} \mp \frac{V_{Aj}}{2\rho} \langle z_i^{\pm} z_k^{\pm*} \rangle \frac{\partial \rho}{\partial r_k} \\ & + \frac{1}{\rho} \langle z_j^{\pm*} \nabla_i \bar{P}' + z_i^{\pm} \nabla_j \bar{P}' \rangle + \langle z_j^{\pm*} (\boldsymbol{\Omega} \times \mathbf{z}^{\pm})_i + z_i^{\pm} (\boldsymbol{\Omega} \times \mathbf{z}^{\pm*})_j \rangle. \end{aligned} \quad (\text{A4})$$

Since we are primarily concerned with describing the transport of energy in fluctuations, we will further deal with the equation for the trace of the correlation tensor

$$\begin{aligned} & \frac{\partial R_{ii}^{\pm}}{\partial t} + [(\mathbf{v} \mp \mathbf{V}_A) \cdot \nabla] R_{ii}^{\pm} + R_{ii}^{\pm} \left[ \nabla \cdot \left( \frac{\mathbf{u}}{2} \pm \mathbf{V}_A \right) \right] \\ & + \Pi_{ii}^{\pm} = N L_{ii}^{\pm} + S_{ii}^{\pm}. \end{aligned} \quad (\text{A5})$$

Here and further on, summation over repeated indices is assumed. Introducing the energy difference tensor  $R_{ij}^D \equiv \langle v_i' v_j'^* - b_i' b_j'^* \rangle$  and the cross-correlation tensor  $R_{ij}^{vb} \equiv \langle v_i' b_j'^* - v_j'^* b_i' \rangle$ , we can re-write the trace of the mixing tensor (A4) in the form

$$\begin{aligned} \Pi_{ii}^{\pm} = & - R_{ii}^{Ds} \left[ \nabla \cdot \left( \frac{\mathbf{u}}{2} \pm \mathbf{V}_A \right) \right] + 2(R_{ik}^{Ds} \mp R_{ik}^{vb-a}) \frac{\partial(u_i \pm V_{Ai})}{\partial r_k} \\ & \mp \frac{V_{Ai}}{2\rho} (R_{ki}^{\pm} + R_{ik}^{\pm}) \frac{\partial \rho}{\partial r_k} + \frac{1}{\rho} \langle (z_i^{\pm*} + z_i^{\pm}) \nabla_i \bar{P}' \rangle, \end{aligned} \quad (\text{A6})$$

where  $R_{ij}^{Ds} = (R_{ij}^D + R_{ji}^D)/2$  is the symmetric part of the energy difference tensor and  $R_{ij}^{vb-a} = (R_{ij}^{vb} - R_{ji}^{vb})/2$  is the anti-symmetric part of the cross-correlation tensor. Note that contributions of the last two “Coriolis” terms in Equation (A4) are canceled out in Equation (A6). As discussed by Zhou & Matthaeus (1990), the term  $\langle (z_i^{\pm*} + z_i^{\pm}) \nabla_i \bar{P}' \rangle / \rho$  can be neglected. If the displacement  $\boldsymbol{\zeta} = 0$  then  $R_{ik}^{vb-a} \partial u_i / \partial r_k =$



$\epsilon_m \cdot (\nabla \times \mathbf{u}/\sqrt{4\pi\rho})$ , where  $\epsilon_m = -\langle \mathbf{v}' \times \mathbf{B}' \rangle$  is the mean-induced electric field, and for transverse to  $\mathbf{B}$  and axisymmetric turbulence we have

$$R_{ij}^{\pm} = R_{kk}^{\pm}(\delta_{ij} - \hat{B}_i \hat{B}_j)/2 = \frac{Z_{\pm}^2}{2}(\delta_{ij} - \hat{B}_i \hat{B}_j),$$

where  $Z_{\pm}^2 = \langle |\mathbf{z}^{\pm}|^2 \rangle = R_{ii}^{\pm}(\zeta = 0)$  are the Elsässer energies. Following Breech et al. (2008), we assume  $R_{ij}^{Ds} \approx \sigma_D R_{ij}$ . Then the mixing term takes the form

$$\begin{aligned} \Pi_{ii}^{\pm} &= \sigma_D Z^2 \left[ \frac{\nabla \cdot \mathbf{u}}{2} - \hat{\mathbf{B}} \cdot (\hat{\mathbf{B}} \cdot \nabla)(\mathbf{u} \pm \mathbf{V}_A) \right] \\ &\mp \frac{2\epsilon_m \cdot [\nabla \times (\mathbf{u} \pm \mathbf{V}_A)]}{\sqrt{4\pi\rho}}, \end{aligned}$$

and for  $u \gg V_A$  we get

$$\begin{aligned} \frac{\partial Z_{\pm}^2}{\partial t} + (\mathbf{v} \cdot \nabla) Z_{\pm}^2 + \frac{Z_{\pm}^2}{2} \nabla \cdot \mathbf{u} + \sigma_D Z^2 M \\ \mp \frac{2\epsilon_m \cdot (\nabla \times \mathbf{u})}{\sqrt{4\pi\rho}} = NL^{\pm} + S^{\pm}, \end{aligned} \quad (\text{A7})$$

where  $M = \nabla \cdot \mathbf{u}/2 - \hat{\mathbf{B}} \cdot (\hat{\mathbf{B}} \cdot \nabla)\mathbf{u}$ . Finally, adding and subtracting Equations (A7), we obtain the sought-for equations for  $Z^2 = (Z_+^2 + Z_-^2)/2$  and  $Z^2\sigma_c = (Z_+^2 - Z_-^2)/2$ :

$$\frac{\partial Z^2}{\partial t} + (\mathbf{v} \cdot \nabla) Z^2 + \frac{Z^2}{2} \nabla \cdot \mathbf{u} + \sigma_D Z^2 M = NL_1 + S_1$$

$$\frac{\partial (Z^2\sigma_c)}{\partial t} + (\mathbf{v} \cdot \nabla)(Z^2\sigma_c) + \frac{Z^2\sigma_c}{2} \nabla \cdot \mathbf{u} - \frac{2\epsilon_m \cdot (\nabla \times \mathbf{u})}{\sqrt{4\pi\rho}} = NL_2 + S_2.$$

Note that the nonlinear ( $NL_1$  and  $NL_2$ ) and source ( $S_1$  and  $S_2$ ) terms are modeled separately (see Breech et al. 2008). The equation for the evolution of the correlation length retains the form (12) of Breech et al. (2008). It is easy to show that for the case of isotropic turbulence  $M = \nabla \cdot \mathbf{u}/6$ .

## APPENDIX B

### MOMENTUM AND TOTAL ENERGY EQUATIONS IN THE ROTATING FRAME OF REFERENCE

In the case of transverse to  $\mathbf{B}$  and axisymmetric turbulence, the momentum equation (6) can be re-written as

$$\begin{aligned} \frac{\partial(\rho\mathbf{v})}{\partial t} + \nabla \cdot \left( \rho\mathbf{v}\mathbf{v} - \frac{\eta}{4\pi}\mathbf{B}\mathbf{B} + \bar{P}\mathbf{I} \right) \\ = -\rho \left[ \frac{GM_{\odot}}{r^2}\hat{\mathbf{r}} + 2\Omega \times \mathbf{v} + \Omega \times (\Omega \times \mathbf{r}) \right], \end{aligned} \quad (\text{B1})$$

where  $\eta = 1 + 2\pi\sigma_D\rho Z^2/B^2$  and  $\bar{P} = P + (1 + \sigma_D)\rho Z^2/4 + B^2/8\pi$  is the total pressure. Let us now transform the terms containing the velocity in the rotating frame  $\mathbf{v}$  using the substitution  $\mathbf{v} = \mathbf{u} - \Omega \times \mathbf{r}$ , where  $\mathbf{u}$  is the velocity in the inertial frame. Using the following vector identities  $\nabla \cdot (\mathbf{F}\mathbf{G}) \equiv \mathbf{G}(\nabla \cdot \mathbf{F}) + (\mathbf{F} \cdot \nabla)\mathbf{G}$ ,  $(\mathbf{F} \cdot \nabla)(\Omega \times \mathbf{r}) = \Omega \times \mathbf{F}$ , where  $\mathbf{F}$  and  $\mathbf{G}$  are arbitrary vectors, and  $\nabla \cdot (\Omega \times \mathbf{r}) = 0$ , it can be shown that

$$\begin{aligned} \frac{\partial(\rho\mathbf{v})}{\partial t} + \nabla \cdot (\rho\mathbf{v}\mathbf{v}) + \rho[2\Omega \times \mathbf{v} + \Omega \times (\Omega \times \mathbf{r})] \\ = \frac{\partial(\rho\mathbf{u})}{\partial t} + \nabla \cdot (\rho\mathbf{u}\mathbf{u}) + \rho\Omega \times \mathbf{u}. \end{aligned}$$

Then we obtain the momentum equation in the form

$$\frac{\partial(\rho\mathbf{u})}{\partial t} + \nabla \cdot \left( \rho\mathbf{u}\mathbf{u} - \frac{\eta}{4\pi}\mathbf{B}\mathbf{B} + \bar{P}\mathbf{I} \right) = -\rho \left( \frac{GM_{\odot}}{r^2}\hat{\mathbf{r}} + \Omega \times \mathbf{u} \right), \quad (\text{B2})$$

and making use of Equation (5), a non-conservation form of Equation (B2):

$$\begin{aligned} \rho \left[ \frac{\partial\mathbf{u}}{\partial t} + (\mathbf{v} \cdot \nabla)\mathbf{u} \right] - \frac{1}{4\pi}(\nabla \times \mathbf{B}) \times \mathbf{B} + \nabla \cdot \left[ P + \frac{(1 - \sigma_D)\rho Z^2}{4} \right] \\ + \nabla \cdot \left[ \frac{\sigma_D\rho Z^2}{2}(\mathbf{I} - \hat{\mathbf{B}}\hat{\mathbf{B}}) \right] = -\rho \left( \frac{GM_{\odot}}{r^2}\hat{\mathbf{r}} + \Omega \times \mathbf{u} \right). \end{aligned} \quad (\text{B3})$$

Using Equation (B3), we can derive a conservation equation for the total energy

$$E = \frac{\rho u^2}{2} + \frac{P}{\gamma - 1} + \frac{B^2}{8\pi} - \frac{\rho GM_{\odot}}{r} + \frac{\rho Z^2}{2}. \quad (\text{B4})$$

Carrying out a time derivative on Equation (B4), we find

$$\begin{aligned} \frac{\partial E}{\partial t} &= \left( \frac{u^2}{2} - \frac{GM_{\odot}}{r} + \frac{Z^2}{2} \right) \frac{\partial\rho}{\partial t} + \rho\mathbf{u} \cdot \frac{\partial\mathbf{u}}{\partial t} \\ &+ \frac{1}{\gamma - 1} \frac{\partial P}{\partial t} + \frac{\mathbf{B}}{4\pi} \cdot \frac{\partial\mathbf{B}}{\partial t} + \frac{\rho}{2} \frac{\partial Z^2}{\partial t}. \end{aligned}$$

Making use of Equations (5), (B3), (7), (8), and (10), we obtain after some algebra

$$\frac{\partial E}{\partial t} = -\nabla \cdot \left[ \mathbf{v}E + \mathbf{u}\bar{P} - \frac{\eta\mathbf{B}(\mathbf{u} \cdot \mathbf{B})}{4\pi} \right] - \frac{\mathbf{B}}{4\pi} \cdot (\nabla \times \epsilon_m) + \frac{\rho\dot{E}_{\text{PI}}}{2}. \quad (\text{B5})$$

We should emphasize that although we apply the substitution  $\mathbf{v} = \mathbf{u} - \Omega \times \mathbf{r}$ , which relates the inertial and rotating frame velocities, Equations (B2), (B3), and (B5) are still written in the coordinates rotating with the Sun.

## REFERENCES

- Alazraki, G., & Couturier, P. 1971, *A&A*, **13**, 380  
 Axford, W. I., & McKenzie, J. F. 1992, in *COSPAR Colloquia Ser. 3, Solar Wind Seven*, ed. E. Marsch & R. Schwenn (Oxford: Pergamon), 1  
 Balogh, A., Smith, E. J., Tsurutani, B. T., Southwood, D. J., Forsyth, R. J., & Horbury, T. S. 1995, *Science*, **268**, 1007  
 Barnes, A. 1979, in *Solar System Plasma Physics*, Vol. 1, ed. C. F. Kennel, L. J. Lanzerotti, & E. N. Parker (Amsterdam: North-Holland), 249  
 Barnes, A., Gazis, P. R., & Phillips, J. L. 1995, *Geophys. Res. Lett.*, **22**, 3309  
 Belcher, J. W. 1971, *ApJ*, **168**, 509  
 Belcher, J. W., & Davis, L. 1971, *J. Geophys. Res.*, **76**, 3534  
 Breech, B., Matthaeus, W. H., Cranmer, S. R., Kasper, J. C., & Oughton, S. 2009, *J. Geophys. Res.*, **114**, A09103  
 Breech, B., Matthaeus, W. H., Minnie, J., Bieber, J. W., Oughton, S., Smith, C. W., & Isenberg, P. A. 2008, *J. Geophys. Res.*, **113**, A08105  
 Breech, B., Matthaeus, W. H., Minnie, J., Oughton, S., Parhi, S., Bieber, J. W., & Bavassano, B. 2005, *Geophys. Res. Lett.*, **32**, L06103  
 Bruno, R., & Carbone, V. 2005, *Living Rev. Sol. Phys.*, **2**, 1  
 Canullo, M. V., Costa, A., & Ferro-Fontán, C. 1996, *ApJ*, **462**, 1005  
 Chen, Y., & Hu, Y. Q. 2001, *Solar Phys.*, **199**, 371  
 Chernyshov, A. A., Karelsky, K. V., & Petrosyan, A. S. 2006, *Phys. Plasmas*, **13**, 032304  
 Chernyshov, A. A., Karelsky, K. V., & Petrosyan, A. S. 2007, *Phys. Fluids*, **19**, 055106  
 Cohen, O., et al. 2007, *ApJ*, **654**, L163  
 Cranmer, S. R., Matthaeus, W. H., Breech, B., & Kasper, J. C. 2009, *ApJ*, **702**, 1604

- Dewar, R. L. 1970, *Phys. Fluids*, **13**, 2710
- Elsässer, W. M. 1950, *Phys. Rev.*, **79**, 183
- Esser, R., Leer, E., Habbal, S. R., & Withbroe, G. L. 1986, *J. Geophys. Res.*, **91**, 2950
- Feldman, W. C., Barraclough, B. L., Phillips, J. L., & Wang, Y. M. 1996, *A&A*, **316**, 355
- Galtier, S., Nazarenko, S. V., Newell, A. C., & Pouquet, A. 2000, *J. Plasma Phys.*, **63**, 447
- Gazis, P. R., & Lazarus, A. J. 1982, *Geophys. Res. Lett.*, **9**, 431
- Germano, M., Piomelli, U., Moin, P., & Cabot, W. H. 1991, *Phys. Fluids A*, **3**, 1760
- Goldreich, P., & Sridhar, S. 1995, *ApJ*, **438**, 763
- Goldstein, M. L., Roberts, D. A., & Matthaeus, W. H. 1995, *ARA&A*, **33**, 283
- Gottlieb, S., Shu, C. W., & Tadmor, E. 2001, *SIAM Rev.*, **43**, 89
- Groth, C. P. T., De Zeeuw, D. L., Gombosi, T. I., & Powell, K. G. 2000, *J. Geophys. Res.*, **105**, 25053
- Hayashi, K. 2005, *ApJ*, **161**, 480
- Hollweg, J. V. 1974, *J. Geophys. Res.*, **79**, 3845
- Hollweg, J. V. 1976, *J. Geophys. Res.*, **81**, 1649
- Hollweg, J. V. 1978, *Rev. Geophys. Space Phys.*, **16**, 689
- Hollweg, J. V. 1990, *J. Geophys. Res.*, **95**, 14873
- Hossain, M., Gray, P. C., Pontius, D. H., Matthaeus, W. H., & Oughton, S. 1995, *Phys. Fluids*, **7**, 2886
- Hu, Y. Q., Li, X., & Habbal, S. R. 2003, *J. Geophys. Res.*, **108**, 1378
- Hundhausen, A. J. 1972, *Coronal Expansion and Solar Wind* (Berlin: Springer)
- Isenberg, P. A., Smith, C. W., & Matthaeus, W. H. 2003, *ApJ*, **592**, 564
- Isenberg, P. A., Smith, C. W., Matthaeus, W. H., & Richardson, J. D. 2010, *ApJ*, **719**, 716
- Jacques, S. A. 1977, *ApJ*, **215**, 942
- Jacques, S. A. 1978, *ApJ*, **226**, 632
- Kurganov, A., & Levy, D. 2000, *SIAM J. Sci. Comput.*, **22**, 1461
- Leer, E., Holzer, T. E., & Flå, T. 1982, *Space Sci. Rev.*, **33**, 161
- Lesieur, M., Métais, O., & Comte, P. 2005, *Large-Eddy Simulations of Turbulence* (Cambridge: Cambridge Univ. Press)
- Levy, D., Puppo, G., & Russo, G. 1999, *Math. Modelling Numer. Anal.*, **33**, 547
- Li, B., Li, X., Hu, Y. Q., & Habbal, S. R. 2004, *J. Geophys. Res.*, **109**, A07103
- Linker, J. A., Van Hoven, G., & Schnack, D. D. 1990, *Geophys. Res. Lett.*, **17**, 2281
- Linker, J. A., et al. 1999, *J. Geophys. Res.*, **104**, 9809
- Lionello, R., Linker, J. A., & Mikić, Z. 2009, *ApJ*, **690**, 902
- Marsch, E., Mülhåuser, K.-H., Schwenn, R., Rosenbauer, H., Pilipp, W. G., & Neubauer, F. M. 1982, *J. Geophys. Res.*, **87**, 52
- Marsch, E., & Tu, C. Y. 1989, *J. Plasma Phys.*, **41**, 479
- Marsch, E., & Tu, C.-Y. 1993, *J. Geophys. Res.*, **98**, 21045
- Matthaeus, W. H., Ghosh, S., Oughton, S., & Roberts, D. A. 1996a, *J. Geophys. Res.*, **101**, 7619
- Matthaeus, W. H., & Goldstein, M. L. 1982, *J. Geophys. Res.*, **87**, 6011
- Matthaeus, W. H., Goldstein, M. L., & Lantz, S. R. 1986, *Phys. Fluids*, **29**, 1504
- Matthaeus, W. H., Goldstein, M. L., & Roberts, D. A. 1990, *J. Geophys. Res.*, **95**, 20673
- Matthaeus, W. H., Minnie, J., Breech, B., Parhi, S., Bieber, J. W., & Oughton, S. 2004, *Geophys. Res. Lett.*, **31**, L12803
- Matthaeus, W. H., Oughton, S., Pontius, D. H., & Zhou, Y. 1994, *J. Geophys. Res.*, **99**, 19267
- Matthaeus, W. H., Zank, G. P., & Oughton, S. 1996b, *J. Plasma Phys.*, **56**, 659
- Matthaeus, W. H., Zank, G. P., Smith, C. W., & Oughton, S. 1999, *Phys. Rev. Lett.*, **82**, 3444
- Meyer-Vernet, N. 2007, *Basics of the Solar Wind* (Cambridge: Cambridge Univ. Press)
- Mikić, Z., & Linker, J. A. 1996, in *AIP Conf. Proc. 382, Solar Wind 8 Symposium*, ed. D. Winterhalter, J. T. Gosling, S. R. Habbal, W. S. Kurth, & M. Neugebauer (Melville, NY: AIP), 104
- Munro, R. H., & Jackson, B. V. 1977, *ApJ*, **213**, 874
- Nakamizo, A., Tanaka, T., Kubo, Y., Kamei, S., Shimazu, H., & Shinagawa, H. 2009, *J. Geophys. Res.*, **114**, A07109
- Neugebauer, M., & Snyder, C. W. 1962, *Science*, **138**, 1095
- Parker, E. N. 1958, *ApJ*, **128**, 664
- Parker, E. N. 1960, *ApJ*, **132**, 821
- Pilipp, W. G., Miggenrieder, H., Mülhåuser, K.-H., Rosenbauer, H., & Schwenn, R. 1990, *J. Geophys. Res.*, **95**, 6305
- Phillips, J. L., et al. 1995, *Geophys. Res. Lett.*, **22**, 3301
- Pneuman, G. W., & Kopp, R. A. 1971, *Solar Phys.*, **18**, 258
- Powell, K. G. 1994, *Tech. Rep. ICASE No. 94-24* (Hampton, VA: Institute for Computer Applications in Science and Engineering)
- Riley, P., Linker, J. A., & Mikić, Z. 2001, *J. Geophys. Res.*, **106**, 15889
- Roussev, I. I., et al. 2003, *ApJ*, **595**, L57
- Scime, E. E., Badeau, A. E., & Littleton, J. E. 1999, *J. Geophys. Res.*, **26**, 2129
- Scudder, J. D., & Olbert, S. 1979, *J. Geophys. Res.*, **84**, 2755
- Shimomura, Y. 1991, *Phys. Fluids A*, **3**, 3098
- Sittler, E. C., & Scudder, J. D. 1980, *J. Geophys. Res.*, **85**, 5131
- Smith, C. W., Isenberg, P. A., Matthaeus, W. H., & Richardson, J. D. 2006, *ApJ*, **638**, 508
- Smith, C. W., Isenberg, P. A., Matthaeus, W. H., Richardson, J. D., Oughton, S., & Zank, G. P. 2004, in *AIP Conf. Proc. 719, Physics of the Outer Heliosphere*, ed. V. Florinsky, N. V. Pogorelov, & G. P. Zank (Melville, NY: AIP), 359
- Smith, C. W., Matthaeus, W. H., Zank, G. P., Ness, N. F., Oughton, S., & Richardson, J. D. 2001, *J. Geophys. Res.*, **106**, 8253
- Smith, E. J., & Wolfe, J. H. 1979, *Space Sci. Rev.*, **23**, 217
- Spitzer, L., & Härm, R. 1953, *Phys. Rev.*, **89**, 977
- Steinolfson, R. S., Suess, S. T., & Wu, S. T. 1982, *ApJ*, **255**, 730
- Totten, T. L., Freeman, J. W., & Arya, S. 1995, *J. Geophys. Res.*, **100**, 13
- Tu, C. Y., & Marsch, E. 1993, *J. Geophys. Res.*, **98**, 1257
- Tu, C. Y., & Marsch, E. 1995, *Space Sci. Rev.*, **73**, 1
- Unti, T. W. J., & Neugebauer, M. 1968, *Phys. Fluids*, **11**, 563
- Usmanov, A. V. 1993a, *Solar Phys.*, **146**, 377
- Usmanov, A. V. 1993b, *Solar Phys.*, **148**, 371
- Usmanov, A. V. 1996, in *AIP Conf. Proc. 382, Solar Wind 8 Conference*, ed. D. Winterhalter, J. T. Gosling, S. R. Habbal, W. S. Kurth, & M. Neugebauer (Melville, NY: AIP), 141
- Usmanov, A. V., & Goldstein, M. L. 2003, *J. Geophys. Res.*, **108**, 1354
- Usmanov, A. V., & Goldstein, M. L. 2006, *J. Geophys. Res.*, **111**, A07101
- Usmanov, A. V., Goldstein, M. L., Besser, B. P., & Fritzer, J. M. 2000, *J. Geophys. Res.*, **105**, 12675
- Verma, M. K. 1996, *J. Geophys. Res.*, **101**, 27549
- Wang, Y. M. 1993, *ApJ*, **410**, L123
- Wang, Y. M., & Sheeley, N. R. J. 1990, *ApJ*, **355**, 726
- Wang, Y. M., Sheeley, N. R. J., Phillips, J. L., & Goldstein, B. E. 1997, *ApJ*, **488**, L51
- Whang, Y. C. 1998, *J. Geophys. Res.*, **103**, 17419
- Williams, L. L., Zank, G. P., & Matthaeus, W. H. 1995, *J. Geophys. Res.*, **100**, 17059
- Yokoi, N. 2010, arXiv:1005.2762
- Yokoi, N., Rubinstein, R., Yoshizawa, A., & Hamba, F. 2008, *J. Turbul.*, **9**, 1
- Yoshizawa, A. 1992, *Phys. Rev. A*, **46**, 3292
- Zank, G. P., & Matthaeus, W. H. 1992, *J. Geophys. Res.*, **97**, 17189
- Zank, G. P., Matthaeus, W. H., & Smith, C. W. 1996, *J. Geophys. Res.*, **101**, 17093
- Zhou, Y., & Matthaeus, W. H. 1990, *J. Geophys. Res.*, **95**, 10291